

## STRUCTURAL PARAMETERS OF THIN AND THICK DISKS IN EDGE-ON DISK GALAXIES

PETER YOACHIM<sup>1</sup> & JULIANNE J. DALCANTON<sup>2,3</sup>

Department of Astronomy, University of Washington, Box 351580, Seattle WA, 98195  
*Draft version June 29, 2021*

### ABSTRACT

We analyze the global structure of 34 late-type, edge-on, undisturbed, disk galaxies spanning a wide range of mass. We measure structural parameters for the galaxies using two-dimensional least-squares fitting to our *R*-band photometry. The fits require both a thick and a thin disk to adequately fit the data. The thick disks have larger scale heights and longer scale lengths than the embedded thin disks, by factors of  $\sim 2$  and  $\sim 1.25$ , respectively. The observed structural parameters agree well with the properties of thick and thin disks derived from star counts in the Milky Way and from resolved stellar populations in nearby galaxies. We find that massive galaxies' luminosities are dominated by the thin disk. However, in low mass galaxies ( $V_c \lesssim 120 \text{ km s}^{-1}$ ), thick disk stars contribute nearly half of the luminosity and dominate the stellar mass. Thus, although low mass dwarf galaxies appear blue, the majority of their stars are probably quite old.

Our data are most easily explained by a formation scenario where the thick disk is assembled through direct accretion of stellar material from merging satellites while the thin disk is formed from accreted gas. The baryonic fraction in the thin disk therefore constrains the gas-richness of the merging pre-galactic fragments. If we include the mass in HI as part of the thin disk, the thick disk contains  $\lesssim 10\%$  of the baryons in high mass galaxies, and  $\sim 25 - 30\%$  of the baryons in low-mass galaxies. Our data therefore indicate that the fragments were quite gas rich at the time of merging ( $f_{\text{gas}} = 75 - 90\%$ ). However, because low mass galaxies have a smaller fraction of baryons in their thin disks, the pre-galactic fragments from which they assembled must have been systematically more gas poor. We believe this trend results from increased outflow due to supernova-driven winds in the lower mass pre-galactic fragments. We estimate that  $\sim 60\%$  of the total baryonic mass in these systems was lost due to outflows. Pushing the episode of significant winds to early times allows the mass-metallicity relationship for disks to be established early, before the main disk is assembled, and obviates the difficulty in driving winds from diffuse disks with low star formation efficiencies. We discuss other implications of this scenario for solving the G-dwarf problem, for predicting abundance trends in thick disks, and for removing discrepancies between semi-analytic galaxy formation models and the observed colors of low mass galaxies.

*Subject headings:* galaxies: formation — galaxies: structure

### 1. INTRODUCTION

The structure of galactic disks provides strong constraints on their formation and evolution. Spiral galaxies have long been recognized to contain several distinct populations of stars (e.g., disks, bulges and halos), each with distinct chemical and kinematic properties that capture unique epochs in the formation of the galaxy. Observations of the Milky Way and a wide range of other galaxies have revealed the need for yet another component, namely, a thick stellar disk. Originally detected as an excess of light at high galactic latitudes in deep surface photometry of early-type galaxies (Burstein 1979; Tsikoudi 1979), a thick disk was later revealed in the Milky Way using star counts (Gilmore & Reid 1983).

The properties of the Milky Way's thick disk have revealed many differences from the thin disk. Structurally, the Milky Way's thick disk has a significantly larger scale height than the thin disk, as its name implies (for reviews see Reid & Majewski 1993; Buser et al. 1999; Norris 1999, and references therein). It also may have a somewhat longer scale length (Robin et al.

1996; Ojha 2001; Chen et al. 2001; Larsen & Humphreys 2003). Thick disk stars are older and more metal-poor than stars in the thin disk (e.g. Reid & Majewski 1993; Chiba & Beers 2000). They are also significantly enhanced in  $\alpha$ -elements, compared to thin disk stars of comparable iron abundance (Fuhrmann 1998; Prochaska et al. 2000; Tautvaišienė et al. 2001; Bensby et al. 2003; Feltzing et al. 2003; Mishenina et al. 2004; Brewer & Carney 2004; Bensby et al. 2005). Kinematically, Milky Way thick disk stars have both larger velocity dispersions and slower net rotation than stars in the thin disk (Nissen 1995; Chiba & Beers 2000; Gilmore et al. 2002; Soubiran et al. 2003; Parker et al. 2004).

For many years, however, it remained unclear whether the thick disk was a truly distinct component of the Milky Way, or whether it was only an older, metal-poor extension of the thin disk, as might be created by steady vertical heating over the lifetime of the Galaxy (e.g., Dove & Thronson 1993). Over the past five years, conclusive evidence that the thick disk is indeed distinct from the thin disk has come from a series of detailed chemical abundance studies. Stars with thick disk kinematics show significant alpha-enhancement compared to thin disk stars with identical iron abundances, thus form-

<sup>1</sup> e-mail address:

<sup>2</sup> Alfred P. Sloan Foundation Fellow

<sup>3</sup> e-mail address:

ing a separate parallel sequence in a plot of  $[\alpha/\text{H}]$  vs  $[\text{Fe}/\text{H}]$  (see the recent review by Feltzing et al. 2004). Studies of resolved stars in nearby galaxies also find a thick disk of old red giant branch stars whose lack of metallicity gradient cannot be explained by steady vertical heating (Seth et al. 2005; Mould 2005).

Three general classes of formation mechanisms have been proposed to explain the properties of the Milky Way thick disk. In the first, a previously thin disk is dynamically heated to form a thick disk, after which a new thin disk forms (Quinn et al. 1993; Velazquez & White 1999; Robin et al. 1996; Chen et al. 2001). In the second, the thick disk forms directly from gas at a large scale height, possibly during a largely monolithic protogalactic collapse (Eggen et al. 1962; Gilmore & Wyse 1986; Norris & Ryan 1991; Burkert et al. 1992; Kroupa 2002; Fuhrmann 2004; Brook et al. 2004). In the third, the thick disk forms from a series of minor-merger events which directly deposit stars at large scale heights (Statler 1988; Abadi et al. 2003). Recent cosmological simulations have suggested a more complicated origin. Disk galaxy simulations by Abadi et al. (2003) find a thick disk which is composed primarily of tidal debris from disrupted satellites while comparable simulations by Brook et al. (2004) find that thick disk stars form during a period of chaotic mergers of gas-rich building blocks. Recent kinematic measurements favor scenarios where mergers play a significant role in thick disk formation (Gilmore et al. 2002; Yoachim & Dalcanton 2005).

While all of the above scenarios are viable explanations for the origin of the Milky Way, the structural parameters of thin and thick disk components in a wide range of galaxies can help distinguish among these formation scenarios. Unfortunately, the measurements required to characterize thick disks are difficult to make outside the Milky Way. The Milky Way thick disk provides less than 10% of the local stellar density (Buser et al. 1999), and this faintness hampers detailed study of comparable extragalactic thick disks. To date, thick disk structural properties have been measured only in a small number of galaxies (Seth et al. 2005; Pohlen et al. 2004; van Dokkum et al. 1994; Morrison et al. 1997; Neeser et al. 2002; Abe et al. 1999; Wu et al. 2002; de Grijs & van der Kruit 1996; de Grijs & Peletier 1997, see Table 2 below). These studies analyze galaxies in the edge-on orientation, which allows clear delineation between regions where thin and thick disk stars dominate the flux. The edge-on orientation also allows line of sight integrations of faint stellar populations to reach detectable levels.

In this paper, we analyze a large sample of edge-on galaxies and decompose them into thick and thin disk components. Analysis of  $B$ ,  $R$ , &  $K_s$  photometry and color maps has previously revealed that these galaxies are surrounded by a flattened faint red envelope, with properties very similar to the Milky Way thick disk (Dalcanton & Bernstein 2002). We now use a full 2-dimensional fitting procedure capable of simultaneously fitting the thick and thin disk light distributions to derive their full structural parameters.

### 1.1. Galaxy Sample

The sample used in this paper was drawn from the optical and infrared imaging found in Dalcanton & Bernstein

TABLE 1  
GALAXIES REJECTED FROM THE 2-DISK  $R$ -BAND FITTING

FGC(E)	Reason for rejection
51	Large central knot
84	Spiral arms visible
143	Bright central star-forming region
442	Spiral arms visible
256	Thin disk below seeing limit, fits did not converge
1863	Large warp, bright foreground stars
1945	Fits did not converge, possibly spiral arms
1971	Polar ring galaxy
2217	Large bulge component
2367	Spiral arms visible
2264	Fits did not converge, scattered light problem
2292	Thin disk below seeing limit, bright foreground stars
E1440	Asymmetric disk
E1447	No velocity data
E1619	Large bulge component

(2000, hereafter Paper I). Briefly, our sample of edge-on bulgeless galaxies was initially selected from the Flat Galaxy Catalog (FGC) of Karachentsev et al. (1993), a catalog of 4455 edge-on galaxies with axial ratios greater than 7 and major axis lengths greater than  $0.6'$ . The color maps and initial detections of the thick disks in 47 galaxies were presented in Dalcanton & Bernstein (2002, hereafter Paper II).

Not all galaxies from Paper I have been included in the analysis presented here. We have excluded several of the more massive galaxies with sizable bulge components that could not be adequately masked or modeled. We likewise eliminated several low mass galaxies with bright central star clusters for similar reasons. We have also removed any galaxies that have either significant warps or visible spiral arms (i.e., that were not viewed perfectly edge-on), as these systems are poorly modeled by our fitting procedure. Finally, we eliminated galaxies whose surface brightness profiles would be severely affected by atmospheric seeing. A full list of the 15 excluded galaxies are listed in Table 1, leaving a sample of 34 galaxies suitable for decomposing into thick and thin components. When possible, we have used distances listed in Karachentsev et al. (2000) derived from a local flow model. Otherwise we use the galaxy's redshift corrected for the motion of the Local Group (Yahil et al. 1977), assuming a Hubble Constant of  $H_0 = 70 \text{ km s}^{-1} \text{ Mpc}^{-1}$ .

## 2. 2D FITTING

### 2.1. Galaxy Models

The distinctive vertical color gradients identified in Paper II suggest that the stellar population above the galaxies' midplanes is different from the one within it. We assume this change is due to the existence of two distinct stellar populations analogous to the MW's thick and thin disks. Our 2-dimensional fitting procedure attempts to decouple these two populations to measure their scale heights, scale lengths, and luminosities.

We model the surface brightness of each disk component as a radially exponential disk. We adopt the luminosity density  $\mathcal{L}$  of each disk component to be

$$\mathcal{L}(R, z) = \mathcal{L}_0 e^{-R/h_R} f(z) \quad (1)$$

where  $(R, z)$  are cylindrical coordinates,  $\mathcal{L}_0$  is the central

luminosity density,  $h_R$  is the radial scale length, and  $f(z)$  is a function describing the vertical distribution of stars.

Throughout, we adopt a generalized vertical distribution

$$f(z) = \operatorname{sech}^{2/N}(Nz/z_0) \quad (2)$$

where  $z_0$  is the vertical scale height and  $N$  is a parameter controlling the shape of the profile near the midplane. For appropriate choices of  $N$ , this equation can reproduce many popular choices for the vertical distribution of star light. With  $N = 1$  Equation 2 becomes the expected form for a self-gravitating isothermal sheet (Spitzer 1942; van der Kruit & Searle 1981a,b, 1982). When  $N \rightarrow \infty$ , Equation 2 reduces to  $f(z) \propto e^{-z/h_z}$ , where  $h_z = z_0/2$ . Previous fits to the vertical distribution suggest that an intermediate value of  $N = 2$  is a better model of galaxy disks (van der Kruit 1988), as expected for the superposition of several populations with a range of vertical velocity dispersions (de Grijs & van der Kruit 1996). However, different values of  $N$  only produce differences near the galaxy midplane, and all share exponentially declining profiles at large radii.

When fitting a thick plus thin disk model, we preferentially use  $N = 1$  for both components because of its physical motivation. We note that since our main goal is not to model galaxies near their midplane where these functions have their largest differences, our results are not particularly sensitive to the choice of model. To permit comparisons to previous work, we also derive single disk fits to our sample using Equation 2 without a fixed  $N$ , allowing the shape of the vertical profile to vary to best fit the data.

To translate the adopted luminosity density into the observed surface brightness distribution, we assume that the disks are viewed perfectly edge-on. Other authors have demonstrated that slight deviations from  $i = 90^\circ$  have minimal impact on the derived structural parameters (e.g., van der Kruit & Searle 1981b; de Grijs et al. 1997). We also assume that scale heights are independent of projected radius for late-type galaxies, as found by van der Kruit & Searle (1981b); Bizyaev & Mitronova (2002); de Grijs & Peletier (1997); Shaw & Gilmore (1990). With the above assumptions, the model edge-on disk surface brightness is given by

$$\Sigma(R, z) = \Sigma_{0,0}(R/h_R)K_1(R/h_R)f(z) \quad (3)$$

where  $K_1$  is a modified Bessel function of the first order,  $\Sigma_{0,0}$  is the edge-on peak surface brightness ( $\Sigma_{0,0} = 2h_R\mathcal{L}_0$ ), and  $R$  is now the projected radius along the major axis. The face-on surface brightness of such a disk is  $\Sigma(R) = \Sigma_0 e^{-R/h}$  with  $\Sigma_0 = 2z_0\mathcal{L}_0$ . Throughout, we convert our edge-on peak surface brightnesses to magnitudes using  $\mu(0, 0) = m_{zp} - 2.5\log(\Sigma_{0,0})$  where  $m_{zp}$  is the photometric zero point from Paper I. The face-on central surface brightness can then be calculated as  $\mu_0 = \mu(0, 0) - 2.5\log(z_0/h_R)$ . The conversion between the edge-on and face-on orientation assumes that disks are optically thin at any orientation, an assumption that is obviously not true for massive galaxies with dust lanes. However, we correct for this effect later in §4.3. We do not model any possible disk truncation, as this is a small effect seen only in the region  $R > 3h_R$  (van der Kruit & Searle 1981b; Kregel & van der Kruit 2004; Pohlen et al. 2000).

Our sample of galaxies was initially selected to be “pure disk” systems, and thus there are very few galaxies which possess a prominent bulge component. We therefore do not attempt to decompose a bulge component from the surface brightness distribution and simply reject galaxies with significant bulges from the sample (Table 1).

We have tested if the profiles described by Equation 2 could be significantly affected by seeing. We convolved model images with a two-dimensional circular Gaussian kernel to simulate the atmosphere’s effect. We found that this step, in general, was unnecessary. Unconvolved fits differed from convolved fits only for the most distant galaxies. Several of these galaxies have been eliminated from the sample, as listed in Table 1.

## 2.2. Fitting Method

We use Levenberg-Marquardt least squares fitting of the galaxy images to find the best parameters for the models described in §2.1. Before fitting, the images of the galaxies are sky-subtracted and foreground stars and background galaxies are generously masked (see Paper II). The images are cropped at  $R \sim 4h_R$  to speed computation time. Our tests have shown that the fits are insensitive to the exact cropping, causing variations in individual parameters of only a few percent. The cropping also reduces the chance that our fits could be biased by warps or flaring of the disks at large radii.

Following the technique of Kregel et al. (2002), we weight each pixel by the inverse of the model surface brightness distribution at that pixel. By using the model rather than the data to determine the weighting, we eliminate the bias of overweighting positive noise spikes. This weighting scheme places large amounts of weight on the lowest signal-to-noise pixels, ensuring that regions of low surface brightness (i.e., where a faint thick disk could be detected) receive adequate weighting. To prevent the fit from being overwhelmed by regions with low signal-to-noise, we set the weight to zero beyond the  $1-\sigma$  noise contour, defined as where the model falls below the standard deviation of the background. Due to the low signal-to-noise ratio in the  $K_s$  band data, these images were clipped at the  $1/2-\sigma$  level to ensure that an adequate number of pixels were included in the fit. Each fit was iterated four times to ensure convergence of the model parameters and weighting scheme. Fits were performed using pixel coordinates and counts, then converted to arcseconds and magnitudes using the calibrations in Paper I.

It is common practice when fitting models to edge-on galaxies to crop out regions near the midplane of the disk (e.e., Kregel et al. 2002; de Jong 1996; Bizyaev & Mitronova 2002). Cropping avoids the hard-to-model effects of dust lanes, bulges, and star forming regions. The color maps of our galaxies imply that galaxies rotating at speeds less than  $120 \text{ km s}^{-1}$  do not contain concentrated central dust lanes (Dalcanton et al. 2004). For more massive galaxies, our weighting procedure ensures that any midplane structure receives a minimal amount of weighting when calculating the goodness-of-fit  $\chi^2$ . We chose to fit models both with and without the midplane cropping to quantify the systematic uncertainties introduced by midplane structure.

We begin by fitting single disk models to all three  $B$ ,

$R$ , and,  $K_s$  images, holding the galaxy position and rotation fixed. We then fit 2-component models to the images, allowing the offsets and rotation to vary, but constraining all components to have the same center and orientation. For this second step, we use only the  $R$ -band images due to their high signal-to-noise. Ideally, we would perform the 2-disk decomposition in the  $K_s$  band which best represents the smooth stellar distribution and is least effected by dust. However, due to the bright infrared sky, the NIR images are lower signal-to-noise and cannot reach to faint regions where a thick disk would dominate. The  $R$ -band therefore represents the best compromise between reaching faint regions of the galaxies while minimizing the effects of dust extinction and bright star forming regions.

When fitting a single disk with only three free parameters, our procedure converges to the same  $\chi^2$  minima given any reasonable initial guesses. However, for multiple component models, which have up to 10 free parameters, we find that fits often converge to local minima rather than to the global minimum. To ensure we find the global minimum when fitting multiple components, we fit each galaxy using up to 50 unique initial parameter guesses, following Wu et al. (2002). The initial parameters for each galaxy model were randomly varied up to  $\pm 50\%$  to ensure we cast a large net in parameter space.

The formal parameter uncertainties that result from our fits are not meaningful because we used a weighting scheme that is not based on the actual pixel uncertainties. Even if we did minimize  $\chi^2$  using formal pixel errors, our returned uncertainties would be much too low. The  $\chi^2$  formalism requires residuals to be Gaussian, which is rarely the case when fitting nearby galaxies. The situation is comparable to trying to model Mount Rainier as a cone—you can do it, but the residuals will be dominated by real physical structures and not random Gaussian measurement errors. In the case of spiral galaxies, real substructure exists in the form of spiral arms, dust lanes, regions of active star formation, warps, flares, HII regions, etc. As an alternative assessment of the systematic errors which are likely to dominate our uncertainties, we fit a series of models using a variety of different weighting and masking schemes (Table 4) and quote the median result for each parameter. We then adopt the full range of convergent models for each parameter as a measure of the inherent systematic uncertainties. The resulting uncertainties are 2-100 times greater than our formal  $\chi^2$  uncertainties, confirming that systematic errors dominate our uncertainties.

### 2.3. Tests on Artificial Images

To assess the reliability of the 2-disk decompositions, we created a set of 100 artificial galaxies. We adopted the surface brightness profile in Equation 2 with an  $N = 1$  vertical distribution for both a thick and thin component, and varied the structural parameters of the disks within ranges similar to our sample galaxies (for the thin disk:  $20.7 \text{ mag}/\square'' < \mu(0,0) < 22.7 \text{ mag}/\square''$ ,  $2.5'' < h_R < 19.4''$ ,  $0.6'' < z_0 < 3.6''$ ; and the thick disk had parameters in the range:  $21.4 \text{ mag}/\square'' < \mu(0,0) < 24.2 \text{ mag}/\square''$ ,  $1.5'' < h_R < 51.2''$ ,  $1.4'' < z_0 < 20''$ ). The model galaxies were convolved with a circular Gaussian with  $1''$  FWHM, typical of the seeing for the observations. We then added read noise, sky noise, and Poisson noise to the simulated

galaxies, with amplitudes chosen to mimic our  $R$ -band data. The galaxy images were rotated up to 2 degrees and offset up to 2 pixels ( $0.5''$ ) from the image center. We then fit the galaxies with the two disk models, with and without seeing corrections. We assume  $N = 1$  and use the same spread of initial parameter guesses as described in §2.2.

Of the 100 simulated galaxies, only three fits failed to converge. 90% of the scale lengths are recovered to within  $\pm 2\%$  of the input value, with all of the results converging within  $\pm 10\%$ . 90% of the scale heights are recovered within  $\pm 3\%$  of the input value with all results within  $\pm 12\%$ . 90% of the central surface brightnesses converge to within 0.09 mags of the correct result. The orientations were always correct to within 0.1 degrees, with a median error less than 1%. All of the spatial offsets were within 1 pixel of the correct position. There were no systematic trends in the size of the errors versus galaxy properties. The high accuracy of these fits indicates that we are not limited by pixel noise in our fits. However, since our model was a perfect match to the input data, this correspondence is not surprising.

We tested models that did not make a seeing correction convolution and found the fits still returned scale lengths and heights that were accurate to  $< 0.2''$ , as long as  $z_0 > 1''$ . The majority of our observed galaxies do have  $z_0 > 1''$ , and thus we do not account for seeing in our fits. This result is consistent with the analysis of de Grijs et al. (1997) who find that for an exponential vertical profile, convolution is unnecessary when the seeing FWHM  $\leq 0.6h_z$ .

In addition to testing our ability to recover the parameters of a known model, we also tested our ability to correctly measure the structural parameters when using an incorrect function for the vertical light distribution. Specifically, we fit an  $N = 2$  model instead of the correct  $N = 1$  vertical profile to each disk. These fits returned results similar to the fits using the correct model, and the resulting scale heights and lengths fell within  $\sim 5\%$  of the correct values. This indicates that the galaxy sizes are constrained primarily by light well away from the midplane. The luminosities were more divergent, however, due to the large differences between these models at their midplanes. The  $N = 2$  model was slightly biased towards having over-luminous thick disks (with a few outliers as well), but the majority (70%) of fits were within a factor of 2 of the correct  $L_{\text{thick}}/L_{\text{thin}}$ , despite being fit with the wrong function.

Finally, we also tested our two-disk fitting code on artificial galaxies that had no second thick disk component. In these cases, the fits always converged to extremely faint thick disks ( $< 1\%$  of the thin disk flux) and usually converged to either very large or very small thick disk scale lengths, mimicking either a uniform sky background or a small point source. Overall, these results encourage us to believe that if there are no thick disk components in our data our fitted parameters will diverge to unphysical values.

## 3. SINGLE DISK FITS

Before discussing the results of decomposing the galaxies into two disk components (§4), we discuss the results for fitting single disks to the light distributions. These fits are useful simple descriptions of the galaxies, and the

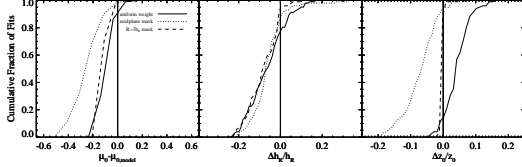


FIG. 1.— Cumulative distributions showing the systematic effects of fitting our galaxies with varying models. All models are compared to a fit using inverse weighting and no masked regions. Fits for all three filters have been combined. The solid curve shows the model which used uniform pixel weighting, while the dotted curve shows the midplane masked model, and the dashed curve shows the  $|R| < 3h_R$  radially masked model.

resulting parameters can be directly compared to previous fits of edge-on and face-on galaxies.

As discussed in §2.2, we quantify our systematic uncertainties using Equation 3 with an  $N = 1$  vertical profile and a variety of weighting and masking techniques resulting in five different fits for each galaxy image. The five fits are: (1) the full galaxy with inverse model weighting as described in §2.2; (2) the full galaxy with uniform weighting to more heavily weight the high signal-to-noise regions; (3) inverse weighting with the midplane region ( $z = \pm z_0$ ) masked; (4) inverse weighting with the outer region  $R > 3h_R$  masked, to eliminate regions where our fit may be affected by unmodeled stellar truncation; and (5) inverse weighting with the high latitude region  $z > 2z_0$  masked to minimize the effect of thick disks. The results of the fits are given in Table 3 for all 3 band passes. The columns show the median edge-on peak surface brightnesses ( $\mu(0,0)$ ), radial scale lengths ( $h_R$ ), and vertical scale parameters ( $z_0$ ) along with their uncertainties. We emphasize again that these are not the formal statistical uncertainties (which are deceptively small), but instead are the full range of values to which the five different fits converged.

In addition to quantifying our uncertainties, the five different fits provide insight into how variations in fitting methods and weighting schemes affect our results. The systematic effects of the different methods are plotted in Figure 1. The most notable features in Figure 1 are the large systematic shifts in the values of  $z_0$  for the single disk fits. Models that are weighted to fit the midplane (e.g. the uniform weighting model), return thinner disks while models that mask the midplane return larger values of  $z_0$ . This effect is present in all three filters, and is exactly what one would expect if disk galaxies were dominated by thin disks at their midplanes and by thick disks with larger scale-heights in the fainter regions. The radially cropped and midplane cropped models result in fits that have fainter central regions and slightly larger scale heights. This is a strong indication that most of our galaxies do not have dust lanes which need to be masked. Cropping regions at high  $z$  has a minimal ( $< 5\%$  change) effect on the fit parameters.

The parameters for the single disk fits listed in Table 3 are plotted in Figures 2, 3, 4, 5, and 6 as a function of the galaxies' circular velocity. In Figure 2, we see the expected trends that more massive galaxies have larger scale heights. We also plot scale heights from the edge-on sample of Kregel et al. (2002) and find that both studies give consistent results for the scale height as a function of

galaxy circular velocity. In Figure 3 we compare our single disk  $R$ -and  $B$ -band fitted scale lengths with the edge-on sample of Kregel et al. (2002) and the face-on measurements of MacArthur et al. (2003); de Jong (1996), and Swaters & Balcells (2002). Overall, we find that lower mass galaxies in the range  $50 < V_c < 120$  have scale lengths wholly consistent with measurements made in comparable face-on systems. However, the highest mass galaxies in our sample have scale lengths that are slightly larger than the average found in previous studies, although they are still within the full range of the comparison data. This offset is worse in the  $B$ -band than in the  $R$ -band, and almost certainly reflects the presence of strong dust lanes in the more massive systems. The higher attenuation towards the central regions of the galaxies will suppress the surface brightness at small radii, leading to apparently larger scale lengths. This offset may also explain why studies of edge-on disks suggest that disks truncate at only 3-4  $h_R$ , whereas face-on studies see no obvious signature of truncation at these radii (Barton & Thompson 1997; Weiner et al. 2001, but see also Pohlen et al. 2002).

In Figure 4 we compare the structural parameters derived in different band passes. We confirm that redder filters converge to shorter scale lengths (Figure 4), a result of the strong radial color gradients seen in both our sample and in face-on galaxies (e.g., Bell & de Jong 2001; MacArthur et al. 2004).

We also find that for galaxies without dust lanes the  $B$ -band scale heights are predominantly thinner than the  $R$ -band. This offset is consistent with the detection of strong vertical color gradients in Paper II, where we found that the midplanes of late-type galaxies were typically bluer than the light above the plane. Somewhat unexpectedly, our  $K$ -band scale heights are also significantly thinner than the  $R$ -band. We believe that this is due to three effects. First, the  $K$ -band data does not reach as deep as the other filters, making it insensitive to the extended thick component. Second, the thinner  $K$ -band scale height may indicate the presence of dust which blocks light from the midplane in optical filters. Finally, there is some indication from studies of resolved stars in nearby galaxies that the  $K$ -band light is not completely dominated by old red giant stars, but instead has a significant contribution from young stars with small scale heights (Seth et al. 2005).

In Figure 5 we plot the axial ratios of our sample galaxies. Overall, our axial ratios are consistent with the work of Bizyaev & Mitronova (2002) who measure flatness parameters for 153 edge-on galaxies imaged in the 2MASS survey and find values of  $h_r/z_0$  ranging from  $\sim 2$  to  $\sim 10$ . Our results are also consistent with the axial ratios from Kregel et al. (2002). We see a slight trend for more massive galaxies to be flatter than less massive galaxies. Other studies have also suggested that low mass, low surface brightness dwarf galaxies are thicker than regular spirals. Estimates of the intrinsic axial ratios of dwarf irregulars range from  $b/a \sim 0.3$  (Hodge & Hitchcock 1966; Binggeli & Popescu 1995) to  $b/a \sim 0.6$  (Sung et al. 1998; Staveley-Smith et al. 1992), all of which are rounder than typical spirals (e.g. Kudrya et al. 1994). We have discussed possible explanations for this behavior in Dalcanton et al. (2004).

Figure 6 shows the edge-on peak surface brightnesses

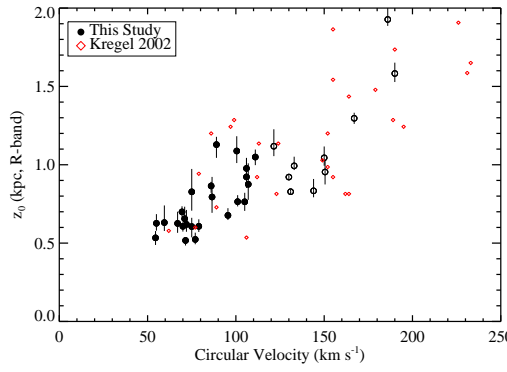


FIG. 2.— Single disk scale heights for the  $R$ -band fits. Galaxies with prominent dust lanes are plotted with open circles. For comparison, we show the  $I$ -band scale heights from the edge-on sample of Kregel et al. (2002), plotted as red diamonds.

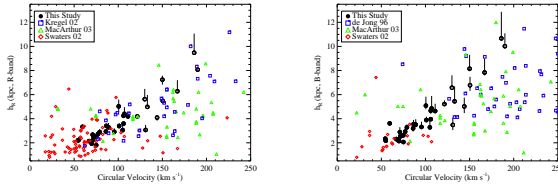


FIG. 3.— Single disk scale lengths for the  $R$ -band (left) and  $B$ -band (right) fits. Galaxies with prominent dust lanes are plotted with open circles. For comparison, we show other single disk fits gathered from the literature. The de Jong (1996) and MacArthur et al. (2003) data are face-on or moderately inclined galaxy samples with the scale lengths measured in the  $R$  and  $B$ -bands (plotted as blue squares and green triangles respectively). The Swaters & Balcells (2002) sample consists of late-type spiral and irregular galaxies with scale lengths measured in the  $R$  and  $B$ -band (plotted as red diamonds). The Kregel et al. (2002) data were measured from edge-on galaxies in the  $I$ -band (plotted as blue squares).

for the one-disk fits. The peak surface brightness of the  $B$ -band data is roughly constant, showing little trend with galaxy mass. However, because the FGC sample was initially selected from the POSS-II survey plates, we would not expect the  $B$ -band surface brightnesses to be below  $\mu \sim 23$  mag/ $\square''$ . On the brighter end, the Freeman law (Freeman 1970) suggests a maximum surface brightness for edge-on disks. Thus, the  $B$ -band peak surface brightnesses must be confined to a limited range. In contrast, we do see increasingly strong trends of surface brightness with mass in the redder filters, and particularly in  $K_s$ . Because the selection criteria for the FGC limited the range of  $B$  surface brightness the observed trends in  $R$  and  $K$  are due to variations in galaxy color with mass. As we will discuss in §4.3, extinction from dust prevents us from being able to reliably convert the edge-on brightnesses to comparable face-on values.

#### 4. TWO DISK FITS

##### 4.1. Need for a Second Component

The traditional signature of thick disks is the presence of excess light at high latitudes after subtracting a single disk component. To demonstrate the expected excess, we subtract the single disk models from the data and sum the residuals (inside the  $1-\sigma$  noise contour) along the major axis. The resulting residuals are plotted in

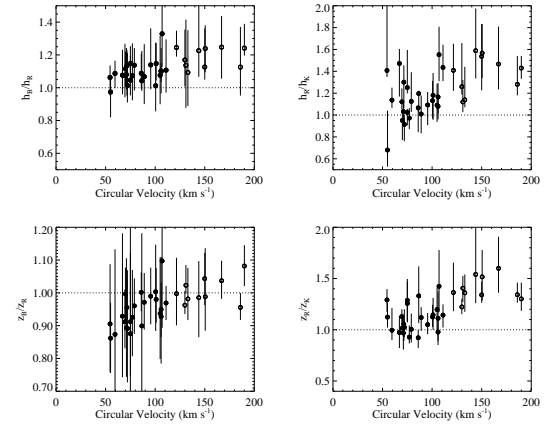


FIG. 4.— Comparison of scale lengths and heights for the single disk fits in different bands. Open symbols are used for galaxies with prominent dust lanes.

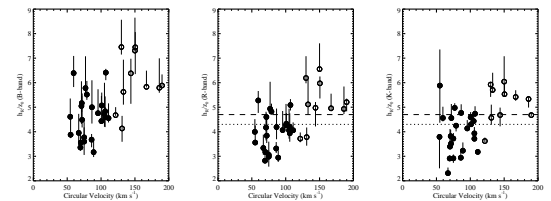


FIG. 5.— Single disk fits showing the flatness ( $h_R/z_0$ ) for each band. Open symbols are used for galaxies with prominent dust lanes. Dotted lines show the average flatness for a sample of 34 galaxies in  $I$ -band presented in Kregel et al. (2002). Dashed lines show the average flatness measured from a sample of 153 galaxies from the Revised Flat Galaxy Catalog imaged by 2MASS in the  $K$ -band and presented in Bilyaev & Mitronova (2002)

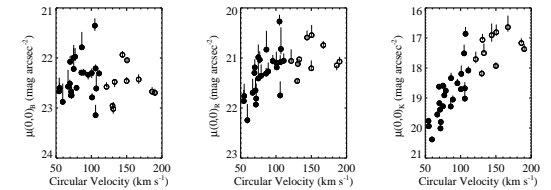


FIG. 6.— Edge-on peak surface brightnesses for the single disk fits. Open symbols are used for galaxies with prominent dust lanes. Points have not been corrected for internal extinction.

Figure 7, and demonstrate that the single disk fits from §3 systematically leave excess flux at high latitudes for all masses of galaxies. We also average the vertical profile residuals across different galaxy mass ranges and find the two disk model is superior to the single disk model in all cases. For a single disk model, we can slightly improve the fit at high  $z$  by allowing the index  $N$  to vary. However, on average, the absolute value of the two-disk model residuals are smaller than the variable  $N$  model at *every* height. By collapsing along the radial direction, we are assuming that any disk components have a nearly constant scale height with radius, as has been found for late type disks in many studies (van der Kruit & Searle 1981b; Bilyaev & Mitronova 2002; de Grijs & Peletier 1997).

These tests show that (1) our galaxies are poorly fit at large  $z$  by the simple  $\text{sech}^2$  model; (2) by leaving the

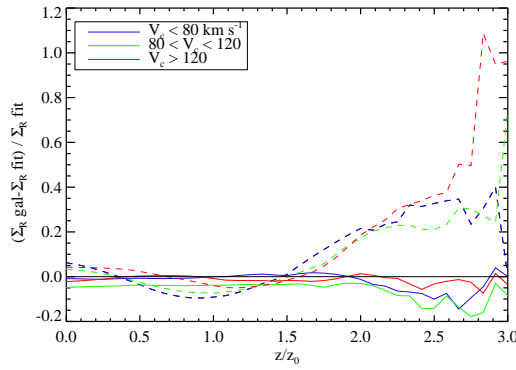


FIG. 7.— *Left:* Residuals collapsed along the radial direction and averaged over galaxies binned by mass. The single disk models (dashed lines) are a very poor fits, leaving large amounts of excess flux at high latitudes. The two disk models (solid lines) do a much better job fitting the vertical light distribution at *all* latitudes and show only a small systematic trend to over-subtract at high  $z$ .

index  $N$  free, we can either fit low  $z$  or high  $z$  regions of the disk well, but not both regions simultaneously; and (3) the two disk model is superior at fitting the vertical profile at all latitudes. We conclude that our galaxies are best modeled by the superposition of two distinct components with unique scale heights.

While we already suspected the galaxies were composed of multiple stellar components based on the observed vertical color gradients and the analogous structures present in the Milky Way, we have now shown that this conclusion can be derived from  $R$ -band images alone. This analysis does not preclude the existence of additional components beyond the two disks considered here, however, although our data do not obviously require them. Our fits also do not demand that the two components trace kinematically and chemically distinct stellar populations that are directly analogous to the thick and thin disks of the Milky Way. On the other hand, when combined with the color gradients observed in Paper II, the data are fairly suggestive of the presence of two genuinely distinct components. We will revisit this issue further in §4.4.1.

Ideally, we could use a statistical goodness-of-fit test to show that a second disk component is required when modeling edge-on galaxies. To establish the need for a thick disk in UGC 7321, Matthews (2000) used an  $F$ -test defined by

$$F = \frac{[\chi^2(1) - \chi^2(2)]/(p - k)}{\chi^2(2)/(n - p)} \quad (4)$$

where  $\chi^2(1)$  characterizes the single disk model with  $k$  free parameters while  $\chi^2(2)$  characterizes the more complex model with  $p$  free parameters and  $n$  total data points. Comparing our two disk models to single disk models with fixed  $N$ , the  $F$ -test favors two disks at the 95% level or higher confidence for 32 of the 34 galaxies, confirming that the two disk model is a better fit than a single disk, as seen in Figure 7. Even if the index  $N$  is allowed to vary, the two disk model is still favored in 31 of the 34 galaxies. Although the  $F$ -test works well for Matthews (2000) when fitting one-dimensional profiles, there are several caveats we must note for our sample.

First, our models do not necessarily minimize the formal  $\chi^2$  value because of our inverse weighting system. Second, the  $F$ -test relies on the  $\chi^2$  formalism and thus assumes all errors are random and Gaussian. As we noted in §2.2, our residuals are definitely non-Gaussian, and therefore the results of any  $F$ -test should be viewed as suggestive but far from conclusive.

#### 4.2. Why Not a Halo?

In addition to modeling the galaxies as a superposition of thick and thin disks, we investigated models composed of a single disk and a “stellar halo” component as advocated by Zibetti et al. (2004). For our halo model, we used a generalized Hubble density distribution (Wu et al. 2002) with the luminosity density

$$\mathcal{L}_{\text{halo}}(r, z) = \frac{\mathcal{L}_{0, \text{halo}}}{\{1 + [r^2 + (z/q)^2]/r_0^2\}^{\gamma/2}} \quad (5)$$

Viewed edge-on, this density distribution projects to the surface brightness profile

$$\Sigma_{\text{halo}}(R, z) = \mathcal{L}_{0, \text{halo}} \sqrt{\pi} \frac{\Gamma[(\gamma - 1)/2]}{\Gamma(\gamma/2)} \times r_0^{\gamma} [r_0^2 + R^2 + (z/q)^2]^{(1-\gamma)/2} \quad (6)$$

where  $\Gamma$  is the standard gamma function

We find our data strongly prefers a second disk component to a halo. Over half of our halo fits converged on very flattened halos ( $q \leq 0.45$ ), essentially reproducing the properties of a thick disk, although one with a radial gradient in scale height. In addition, 40% of the fits converged to halo luminosities that are less than 1% of the disk luminosity, implying that the fitting procedure cannot actually use the new component to improve upon the single disk fits. When unconstrained, the halo exponential parameter  $\gamma$  ran away to very large or small values (producing a uniform background or a compact point source), again implying that a power-law halo is not the appropriate model for the light distribution at high  $z$ .

Using the  $F$ -test defined in §4.1 to compare the two disk fits to 9 free parameters with the disk plus halo fits with 10 free parameters, we found only 11 of the galaxies were better fit with a halo than the second disk. Even when  $\chi^2$  suggested that the halo model was a better fit, the flattening parameter converged to extreme values (less than 0.4, or greater than 1) in 7 of the 11 cases, thus flattening the halo into a more disk-like structure. In those cases, the preference of a halo component may indicate the presence of a radial gradient in disk scale height. In the few cases when a preferred halo fit remained roughly circular, it was because the halo collapsed to fit a small central bulge or star-forming region. Because these regions are bright, they can greatly affect the formal value of  $\chi^2$  and the  $F$ -test will prefer the halo model despite no real improvement in fitting the flux at large scale heights.

The poor results of our attempted halo fitting do not explicitly rule out the presence of a halo at lower surface brightnesses than we can detect in our images. Indeed, a stellar halo like the MW’s would only start to dominate the thick disk component at  $\mu_R \sim 27.5$  mag/ $\square''$  (Morrison et al. 1997) around  $z \sim 10z_0$  (our fits extend to only  $z \sim 3 - 4z_0$ ). In M31 the stellar halo population dominates at a projected radius of

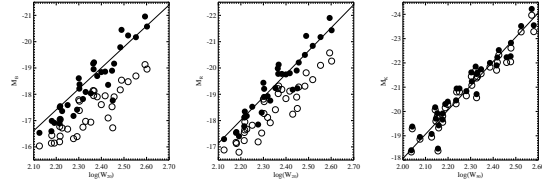


FIG. 8.— Tully Fisher relation derived from the single disk fits. Open circles show points uncorrected for internal extinction while solid circles have been corrected for internal extinction using the method of Tully et al. (1998). Solid lines on the left and middle panel show TF relations from the Hubble Key Project (Sakai et al. 2000). The solid line in the right panel shows the  $K'$  TF-relation of Verheijen (2001). The luminosities for the two disk fits show a comparable offset.

$\sim 30$  kpc and a surface brightness level of  $\mu_V \sim 31$  mag/ $\square''$  (Guhathakurta et al. 2005), and thus comprises  $< 5\%$  of the total stellar luminosity. As before, if a comparable halo component was present in our sample it would be much too faint to be detected in our data.

Zibetti et al. (2004) fit a composite galaxy created by stacking over 1000 edge-on spirals from the Sloan Digital Sky Survey. Using equation 6, they found a slightly flattened halo with  $q = 0.50$  in  $g$ , 0.60 in  $r$  and  $i$ , and 0.70 in  $z$ . There are several reasons we believe the excess light we detect at high latitudes is not equivalent to the halo component discussed by Zibetti et al. (2004): (1) Our  $R$ -band is close to  $r$  and  $i$ , yet when we try to fit a halo component, our values of  $q$  are much lower with a median value of 0.4; (2) The Zibetti et al. (2004) halos only begin to dominate the surface brightness at very large heights ( $z = 16z_{0,s}$ ) beyond our  $1-\sigma$  cropping limit; (3) Zibetti et al. (2004) find that their stellar halo becomes prominent at a surface brightness of  $\mu_r \sim 27$  mag/ $\square''$ , fainter than what we can detect in our individual images.

### 4.3. Dust effects

We have previously found that galaxies in our sample with rotational velocities greater than  $120$  km  $s^{-1}$  host concentrated dust lanes (Dalcanton et al. 2004). We therefore need to consider the effect that dust extinction will have on our fitted parameters. To quantify the amount of extinction in our edge-on sample, we compare the total luminosities of our best fit models to the Hubble Key Project Tully-Fisher relation (Sakai et al. 2000) in Figure 8. We find that all of our galaxies, even those without recognizable dust lanes, lie significantly below the TF-relation for face-on spirals. If we apply the extinction correction of Tully et al. (1998), however, our extinction corrected total luminosities move nicely onto the face-on TF relation.

Their offset from the Tully-Fisher relation implies that our models do not capture all the stellar flux from our galaxies. There are several possible ways dust could influence our fitted parameters to yield lower than expected total luminosities: (1) the peak surface brightnesses could be too low; (2) the scale lengths could be too short; (3) the scale heights could be too small; (4) the vertical profile could appear less peaked than it truly is (e.g., a  $\text{sech}^2$  instead of an exponential); or (5) some combination of the above.

We can say with some certainty that the scale lengths do not appear to be shortened by dust extinction. If any-

thing, Figure 3 shows that our scale lengths are larger than those measured in face-on systems. In a similar fashion, it is unlikely that our scale heights are shortened greatly due to dust, as their bias is likely to have the same sign as the scale lengths. Moreover, our weighting scheme de-emphasizes the midplane region, and our scale height fit is therefore dominated by flux coming from high galactic latitudes. Therefore, any dust distribution which is concentrated along the midplane, or uniformly distributed though the galaxy, should have little to no impact on our fitted value for the scale height. Only a truly pathological dust distribution, such as one having large amounts of dust at high  $z$  compared to the midplane, would skew our scale height parameter to lower values.

Having eliminated biases in the scale height and scale length, we find that dust extinction is most likely affecting our choice of vertical profile and/or the fitted value of the peak surface brightness. Unfortunately, there is a degeneracy between these two parameters which could only be broken if we knew the intrinsic dust distributions in our galaxies. If the dust affects only the midplane region, then the error could be confined to just the vertical distribution, while a more diffuse and vertically uniform dust distribution would lower the central surface brightness but not affect the vertical profile.

We conclude that while our galaxies display clear signs of internal extinction caused by dust, the lost flux will cause us to either pick the wrong vertical profile (which is not of particular importance since we are not concerned with the midplane behavior), and/or underestimate the overall flux normalization as parameterized by the edge-on central surface brightness. However, since the empirical extinction correction of Tully et al. (1998) does an excellent job moving our galaxies onto the TF relation (despite the correction originally not being intended for use on galaxies with extreme inclination angles), we chose to apply this correction to the luminosity of our thin disk component. We do not assume any correction for the extended thick component, since a much smaller fraction of its projected area would be obscured by dust.

### 4.4. Results of Thick + Thin Disk Fits

We now discuss the results of fitting two disk components. We fit a total of six 2-disk models, each with different combinations of  $N = 1$  and  $N = 2$  vertical profiles for the thick and thin components. We also considered models convolved with a  $\sigma = 1''$  circular Gaussian (to model seeing) and models where the midplane ( $\pm z_{0,\text{single}}$ ) is masked (to avoid dust lane contamination). The properties of the models are described in Table 4. We use the inverse-weighting scheme for all the fits, as we found that one disk component always collapses to fit bright midplane structures if more conventional weighting is adopted. As discussed above, we fit the two-disk models only to the  $R$ -band images. Our  $K_s$ -band data does not go deep enough to reliably detect the thick disk component, and the  $B$ -band suffers from dust extinction, is biased towards young stellar populations, and is a poor tracer of the faint red light expected from an old thick disk.

The resulting parameters for the fits are listed in Table 5. For the central value of each parameter we list the median value of convergent  $N = 2$  models. The

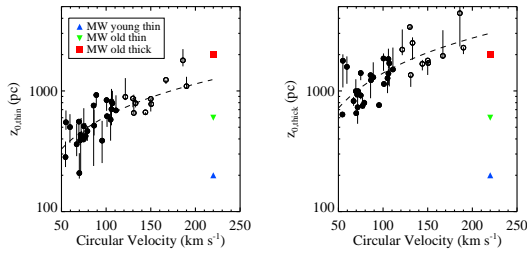


FIG. 9.— Scale heights of thin and thick disks. Values for the Milky Way from Larsen & Humphreys (2003) are plotted for comparison using  $z_0 = 2h_z$  for an exponential vertical profile. Open symbols are used for galaxies with prominent dust lanes. Dashed lines show power-law fits to the data ( $z_{0,thin} = (610 \text{ pc})\left(\frac{V_c}{100 \text{ km s}^{-1}}\right)^{0.90}$  and  $z_{0,thick} = (1400 \text{ pc})\left(\frac{V_c}{100 \text{ km s}^{-1}}\right)^{1.0}$ ). In galaxies that have strong dust lanes, the scale height of the thin disk is likely to be biased towards larger values.

uncertainties are the full range of values to which the different models in Table 5 converged, as discussed in §2.2. We also list the ratio of total luminosities for the model thick and thin disks. The range of luminosity ratios include models with disks having  $N = 1$  or  $N = 2$ . The luminosity ratios are calculated only for flux which falls inside the  $1-\sigma$  noise region (i.e. only the region that was included in the fit). The true luminosity ratios could therefore be different from our quoted values if the disks extend far beyond our detection limits. We have measured the size of this correction by extrapolating the fits and find it can change the luminosity ratios by only 10% at most. The luminosity ratios in Table 5 do not include the extinction corrections derived in §4.3.

#### 4.4.1. Scale heights of the thick and thin disks

The scale heights of our thick and thin disks are plotted in physical units in Figure 9. The scale heights of both the thin and thick disks increase systematically with circular velocity. Fitting power laws to the relations, we find  $z_{0,thin} = (610 \text{ pc})\left(\frac{V_c}{100 \text{ km s}^{-1}}\right)^{0.90}$  and  $z_{0,thick} = (1400 \text{ pc})\left(\frac{V_c}{100 \text{ km s}^{-1}}\right)^{1.0}$  with RMS scatters of 30% in both cases. In general, the scale heights of the two disks bracket the scale height derived for a single disk, as expected.

For massive galaxies with large circular velocities ( $V_c \gtrsim 170 \text{ km/s}$ ), our derived value for the scale height of the thin disk is 2-3 times larger than the MW's thin disk. However, these galaxies have the most prominent dust lanes, which may substantially obscure our view of the thin disk. It is therefore likely that the scale heights of the thin disk may be significantly overestimated in these cases. The plot of  $z_{0,R}/z_{0,K}$  for the single disk fits (Figure 4, lower right) is also consistent with this interpretation. Unfortunately, this limitation is unavoidable until sufficiently deep  $K$ -band data is available.

Figure 10 shows the ratio of the thick to the thin disk scale height  $z_{0,thick}/z_{0,thin}$ . We find a mean ratio of 2.5 with a scatter of 30%. In Figure 11 we show our data along with other thick and thin disk scale heights derived from the literature. For the Milky Way, these scale heights are derived from star counts. For the other literature values, the scale heights are derived either from fitting double exponential profiles to 1-d cuts through

the galaxies or from 2-d fitting similar to the procedure used in this paper. We summarize these other results in Table 2. Figure 11 indicates that our scale height ratios are slightly lower than those measured in other systems ( $z_{0,thick}/z_{0,thin} \sim 3$ ), implying that our derived thick disks may be  $\sim 25\%$  thinner and/or our thin disks are thicker than those derived in other galaxies with other methods. However, our median  $z_{0,thick}/z_{0,thin}$  is very similar to Neeser et al. (2002)'s measurement of the LSB galaxy ESO 342-017, the most comparable galaxy in the literature to galaxies in our sample. These differences may indicate that the thick disks of early type galaxies may be proportionally thicker than those of late type galaxies.

TABLE 2  
THICK DISKS FROM THE LITERATURE

galaxy name	Type	Band	Fitted	$V_c$ (km s $^{-1}$ )	$\frac{z_{0,thick}}{z_{0,thin}}$	$\frac{h_{R,thick}}{h_{R,thin}}$	$\frac{L_{thick}}{L_{thin}}$	Reference
34 galaxies	Sd	<i>R</i>	2-d	55-190	1.6-5.5	0.6-1.6	0.07-7	This study
6 galaxies	Sd	star counts	1-d	67-131	1.7-2.7	-	-	Seth et al. (2005)
ESO 342-017	Scd	<i>R</i>	1-d	127	2.5	1	0.45	Neeser et al. (2002)
IC 5249	Sd	<i>R</i>	1-d	110	3	0.6	-	Abe et al. (1999)
MW	Sbc	star counts	2-d	220	3	1.3	$\sim 0.13$	Larsen & Humphreys (2003)
NGC 6504	Sb	<i>R</i>	1-d	110 <sup>1</sup>	3.9	-	$\sim 0.4$	van Dokkum et al. (1994)
NGC 891	Sb	<i>R</i>	1-d	224	3.5	-	0.12	Morrison et al. (1997)
NGC 4565	Sb	6660 Å	1-d	244	2.2	1.4	-	Wu et al. (2002)
5 galaxies	S0	<i>R</i> and <i>V</i>	2-d	$\sim 130^2$	2.6-5.3	1.7-1.9	0.33-1.0	Pohlen et al. (2004)
NGC4710	S0	<i>R</i>	1-d	147	3.2	-	-	de Grijs & van der Kruit (1996)
NGC4762	S0	<i>R</i>	1-d	110	4.6	-	-	de Grijs & van der Kruit (1996)
Simulation	-	-	-	240	4.7	-	0.35	Abadi et al. (2003)
Simulation	-	-	-	150	2.6	0.63	0.8	Brook et al. (2003)

<sup>1</sup>Estimated from Tully-Fisher relation

<sup>2</sup>Dynamical information only available for 2 of the 5 galaxies

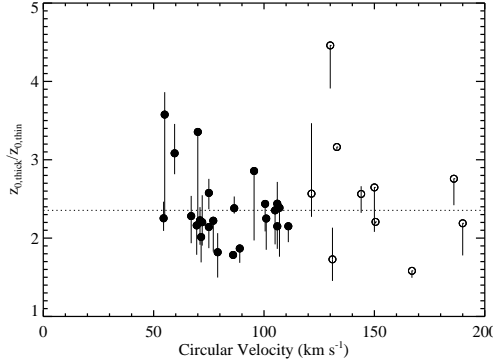


FIG. 10.— Ratios of the scale heights for the thick and thin disks. Error bars represent the full range of ratios to which different models converged. Galaxies with prominent dust lanes are plotted as open circles. The dotted line shows the median value of  $z_{0,\text{thick}}/z_{0,\text{thin}} = 2.35$ .

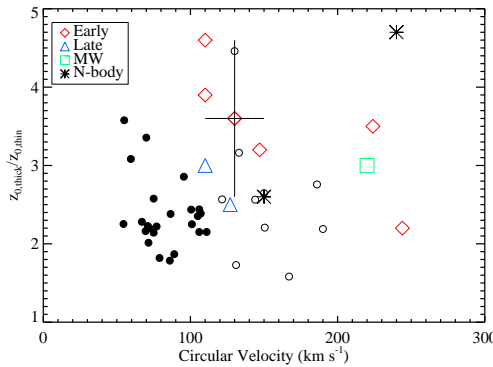


FIG. 11.— Comparison of our scale height ratios to values drawn from the literature. We compare to early-type galaxies (Sb and earlier; red diamonds), late type galaxies (Sc and Sd; blue triangles), the MW (green square), and simulated galaxies. The range of values available for the Pohlen et al. (2004) sample of early type galaxies is plotted as a single point with error bars.

We also do not *a priori* know whether our thick and thin components are strict analogs of any particular component in the disk of the Milky Way, which is usually broken into at least three components; (1) the “young star-forming disk” ( $z_0 \sim 200$  pc) which is dominated by molecular clouds, dust, and massive OB stars; (2) the “old thin disk” ( $z_0 \sim 600$ ); and (3) the “thick disk” ( $z_0 \sim 2$  kpc) (Bahcall & Soneira 1980; Reid & Majewski 1993; Buser et al. 1999; Larsen & Humphreys 2003; Ojha 2001; Chen et al. 2001), which contains  $\sim 15\%$  of the total disk light (Buser et al. 1999; Chen et al. 2001; Larsen & Humphreys 2003).

One possibility is that our thin and thick disks might be analogous to the MW’s young star forming disk and old thin disk, respectively, with no detectable analog of the MW thick disk. However, we do not believe the second component we have fit is an “old-thin” disk. The scale heights of our thin disks are larger than what has previously been measured for thin star forming layers. Matthews (2000) find UGC 7321 has a “young disk” with  $z_0 \approx 185$  pc. Similarly, IC 2531 has a young disk with  $z_0 \sim 134$  pc (Wainscoat et al. 1989) and the MW’s young disk has  $z_0 \sim 200$  pc (Bahcall & Soneira 1980;

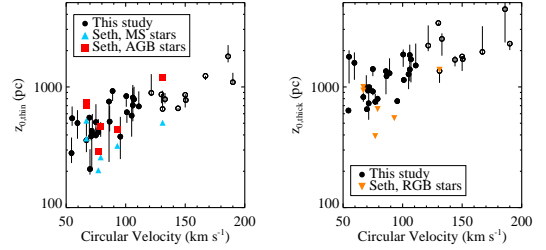


FIG. 12.— Comparison of our results with the scale heights of different stellar populations measured from resolved stars in 6 nearby galaxies (Seth et al. 2005). The component we have identified as the thin disk appears to be intermediate between the scale height of young Main Sequence stars and medium-age Asymptotic Giant Branch stars while our thick disk component is similar to the old Red Giant Branch populations.

Reid & Majewski 1993); (using the conversion that at large scale heights  $z_0 \approx 2h_z$ ). All known young star-forming disks thus have  $z_0 \sim 200$  pc. The only galaxies in our sample that have thin disk scale heights approaching values this small are far less massive than any of the galaxies in the previous studies.

Having ruled out an old thin disk, we now consider the possibility that our second thicker disk component is analogous to the MW’s thick disk. We find strong support for this possibility from studies of resolved stellar populations in similar systems (e.g., Seth et al. 2005; Mould 2005; Tikhonov et al. 2005). In particular, a recent analysis of resolved stellar populations in edge-on galaxies by Seth et al. (2005) separates stars into young Main Sequence (MS), older Asymptotic Giant Branch (AGB), and still older Red Giant Branch (RGB) stars. Seth et al. (2005) find that the younger stellar populations have systematically smaller scale heights than the ancient RGB population. In Figure 12, we compare our thin and thick disk scale heights with the MS, AGB, and RGB scale heights of Seth et al. (2005). We find that our thin disk components have scale heights very similar to the young and intermediate age stellar populations of Seth et al. (2005), while our thick disk components have scale heights similar to, or perhaps slightly larger than, the old RGB populations. Figure 12 supports that what we have labeled the thin disk hosts a young and intermediate age stellar population akin to the thin disk of the Milky Way while what we have labeled as the thick disk traces a different older and redder population, not an extension of the thin disk. When coupled with our observation of strong vertical color gradients (Paper II), and kinematic differences above and at the midplane, we believe there is compelling evidence that the second disk component required by our surface photometry does represent a truly distinct stellar population.

#### 4.4.2. Ratio of scale lengths

Physical values of the thick and thin disk scale lengths are plotted in Figure 13. We see a systematic increase in the radial scale lengths of both disk components with galaxy mass. The data are well fit by  $h_{R,\text{thin}} = (3.4 \text{ kpc})\left(\frac{V_c}{100 \text{ km s}^{-1}}\right)^{1.2}$  and  $h_{R,\text{thick}} = (3.9 \text{ kpc})\left(\frac{V_c}{100 \text{ km s}^{-1}}\right)^{1.0}$  with RMS scatters of 22% and 29% respectively.

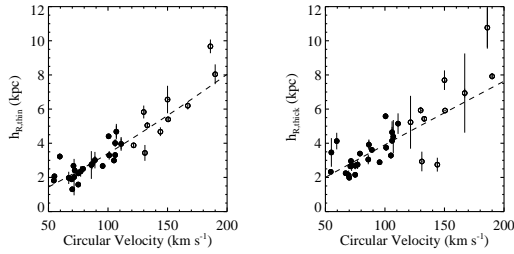


FIG. 13.— Scale lengths of thick and thin disks from the 2-disk fits. The dashed lines show power law fits. Open symbols are used for galaxies with prominent dust lanes. Dashed lines show power-law fits of  $h_{R,\text{thin}} = 3.4(V_c/100 \text{ km s}^{-1})^{1.2}$  kpc and  $h_{R,\text{thick}} = 3.9(V_c/100 \text{ km s}^{-1})^{1.0}$  kpc.

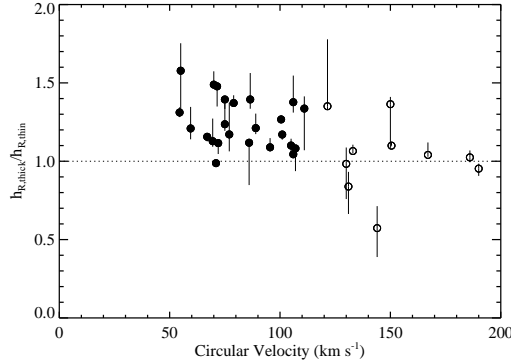


FIG. 14.— Ratios of the scale lengths for the thick and thin disks. The horizontal line indicates where the thin and thick disk components have equal scale lengths. Error bars represent the full range of ratios to which different models converged, and are indicators of our systematic errors. Open symbols are used for galaxies with prominent dust lanes.

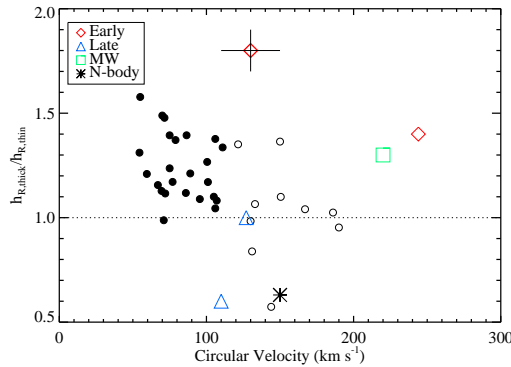


FIG. 15.— Comparison of our scale height ratios to values drawn from the literature. Comparison points are the same as Figure 11.

In Figure 14 we plot the ratio of the thick to thin disk scale lengths. We find that the thick disks have systematically larger scale lengths for all but 5 galaxies. Thick disks with long scale lengths are in excellent agreement with previous thick disk measurements, as shown in Figure 15 where we include data from the literature (Table 2). In all but one measurement of physical (i.e., non-simulated) thick disk scale lengths, the thick disk is found to be slightly longer than the thin disk.

We were initially concerned that this result could be a systematic result of our weighting and masking scheme. For example, if our galactic disks truncate at large radii as found in other edge-on systems (Kregel et al. 2002; Kregel & van der Kruit 2004), then our model fits would converge to have the fainter thick disk dominate at large  $R$ . However, we included a model (Table 4) where the midplane is masked (which also effectively removes regions of the galaxy where disk truncation would be detectable) and still found that the thick disks have longer scale lengths.

We note that there are some limitations in interpreting our scale lengths, particularly for the thin disk. First, the derived radial scale lengths do not necessarily reflect the stellar radial scale length. The thin disk in particular shows a strong radial color gradient, implying a mass-to-light ratio that decreases with increasing radius (see color maps in Paper II). This trend suggests that the radial scale length of the stellar mass should be even smaller for the thin disk, further increasing the ratio  $h_{R,\text{thick}}/h_{R,\text{thin}}$ . We may also have overestimated the scale length of the thin disk if it is affected by dust in a manner similar to the what is observed in our single disk fits (Figure 3 and §4.3). Both of these effects suggest that  $h_{R,\text{thick}}/h_{R,\text{thin}}$  may be even larger than indicated by Figure 14. On the other hand, HI is typically more extended than the optical disk (Swaters et al. 2002; Begum et al. 2005), such that the radial scale length of the baryons in the thin disk may be longer than indicated by  $h_{R,\text{thin}}$ .

#### 4.4.3. Axial ratios of the thick and thin disks

The axial ratios ( $h_R/z_0$ ) for our thick and thin disks are plotted in Figure 16 along with values for the MW thick and thin components for comparison. We find our thick disks have a mean  $h_R/z_0 = 3.4$  with an RMS scatter of 1.7 while the thin disk has a mean value of  $h_R/z_0 = 4.7$  and RMS scatter of 1.8. Our thin disks therefore tend to be comparable to the MW thin disk, but are slightly rounder at low masses, in agreement with other studies (see §3). The axial ratios of the thick disks show a large spread in axial ratios, and are in general comparable to, or slightly thicker than the MW thick disk. However, the radial scale length of the MW is not well constrained since it is determined primarily from star counts near the solar circle. We also note that the thick disk component is drastically rounder than the MW's old thin component, further ruling out the old thin disk as an explanation for our second disk component.

#### 4.4.4. Peak surface brightnesses

The edge-on peak surface brightnesses for our two disk components are plotted in Figure 17. There is a trend for more massive thin disks to have brighter peaks, similar to the trend seen in the single disk fits (Figure 6). The thick disk components show a large amount of scatter in their peak values.

Performing a naive transformation to convert to the face-on orientation, the central surface brightness becomes  $\mu_0 = \mu(0,0) - 2.5\log(z_0/h_R)$ . We find that the average central surface brightness of the thick disk is 0.6 mag/ $\square''$  fainter than the thin disk, implying only  $\sim 35\%$  of the stellar flux in the  $R$ -band would come from the

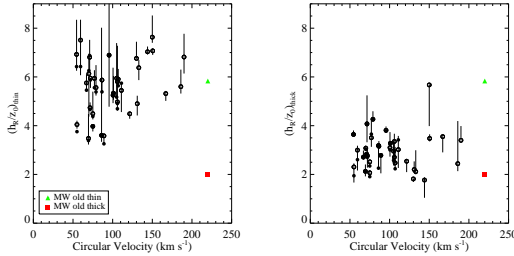


FIG. 16.— Axial ratio ( $h_R/z_0$ ) vs circular velocity for the thin (left) and thick (right) disks. Galaxies with prominent dust lanes are plotted as open circles. The axial ratios of Milky Way disk components are plotted for comparison (Table 2). The axial ratios of our thin and thick disks agree well with the comparable components for the MW.

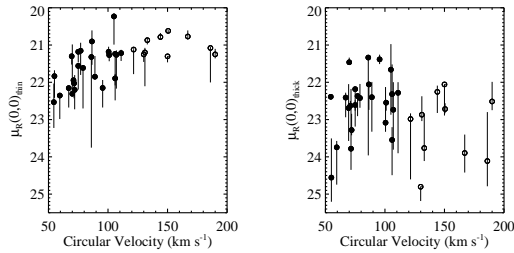


FIG. 17.— Edge-on peak surface brightnesses for the 2-disk fits in the  $R$ -band. Galaxies with prominent dust lanes are plotted as open circles.

thick disk if the galaxies were viewed face-on. In the more massive galaxies, the face-on central surface brightness of the thick disk can be up to 2 mag/□'' fainter than the thin disk. These values do not include corrections made for extinction. Presumably, the thin disk would suffer less extinction when viewed face on, and would further dominate the observed stellar flux. It is therefore not surprising that the thick disk is largely undetected in face-on galaxies.

The total integrated colors of the galaxies will be biased towards the thin disk population as well. After making the extinction corrections in §4.3, we find the total integrated colors of our low mass-galaxies ( $V_c \lesssim 100 \text{ km s}^{-1}$ ) are in the range  $0.5 < B - R < 1$ , much bluer than the thick disk (see Figure 20 below). Using the Bruzual & Charlot (2003) stellar synthesis code, these colors correspond to a stellar population burst with an age of  $\sim 1$  Gyr, or a galaxy with a uniform star formation history. Thus, in spite of the substantial thick disk population, the mean colors of the galaxy reflect only the youngest disk population.

#### 4.4.5. Ratio of luminosities

We now compare the total luminosities of the thick and thin disks (Figure 18). In our raw fits, the luminosity of the thin disk is almost certainly underestimated due to the effects of dust, as shown in §4.3. To correct for dust, we assume that all flux lost from extinction (Figure 8) should be assigned to the thin disk. This correction will give us the most conservative estimate for the contribution of the thick disk to the total stellar luminosity. Figure 18 shows a strong trend with mass (Spearman  $\rho = -0.70, 4.0\sigma$ ). Thick disks of high mass galaxies

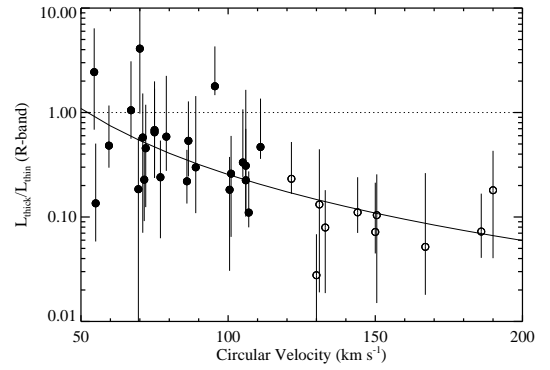


FIG. 18.— Ratio of the total  $R$ -band luminosity of the thick disk compared to the thin disk for the sample galaxies. The thin disk luminosities have been corrected for internal extinction. The dotted line indicates where the thick and thin disks contribute equally to the total luminosity. Error bars show the full range of values from different models, and are indicative of our systematic errors. Galaxies with prominent dust lanes are plotted as open circles. The solid line is a fitted power-law of the form  $L_{\text{thick}}/L_{\text{thin}} = 0.25(V_c/100 \text{ km s}^{-1})^{-2.1}$ .

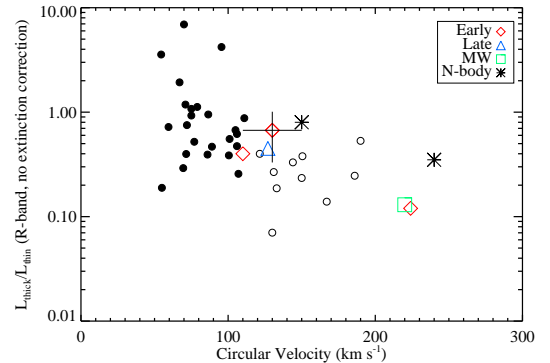


FIG. 19.— Comparison of our luminosity ratios to others in the literature. Comparison points are the same as Figure 11. Unlike Figure 18, we have made no correction of internal extinction to allow for easier comparison with previous studies.

( $V_c > 120 \text{ km s}^{-1}$ ) contribute  $\sim 10\%$  of the total luminosity of the galaxy, while in lower mass systems the thick disk contributes up to  $40\%$  of the total luminosity. This trend can be well represented by the relation  $L_{\text{thick}}/L_{\text{thin}} = 0.25(V_c/100 \text{ km s}^{-1})^{-2.1}$ , shown as a solid line in Figure 18.

We compare our measurements to previous thick disk measurements in Figure 19. Unfortunately, there are few measurements of total disk luminosities in the literature. When possible, we have taken other authors' disk parameters and calculated the resulting total luminosities (see Table 2). For the Milky Way, the local stellar density of thick disk stars has consistently been measured between 4 and 10% of the local thin disk density (e.g., Buser et al. 1999; Chen et al. 2001), which corresponds to a total luminosity ratio of  $\sim 13\%$  for reasonable estimates of scale heights, lengths, and mass-to-light ratios for the two disks. Because the values of  $L_{\text{thick}}/L_{\text{thin}}$  from the literature do not include internal extinction corrections, we compare them to our uncorrected luminosity ratios.

Figure 19 shows that our luminosities compare well with other thick-thin disk systems in the literature. The higher mass galaxies in our sample ( $V_c \sim 140 - 200 \text{ km s}^{-1}$ ) tend to be thin disk dominated with  $L_{\text{thick}}/L_{\text{thin}} \sim 0.1 - 0.2$  (corrected for extinction), like the Milky Way and NGC 891. Intermediate mass galaxies ( $70 < V_c < 100 \text{ km s}^{-1}$ ) have slightly more luminous disks, similar to measurements of ESO 342-017 (Neeser et al. 2002) and S0's (Pohlen et al. 2004). Unfortunately, we cannot find any comparable measurements of thick disks in the low mass systems ( $50 < V_c < 70 \text{ km s}^{-1}$ ) that are thick disk dominated in our sample.

We believe our measurement of the total luminosities are more robust than the measures of the peak surface brightness. Central surface brightnesses depend strongly on the vertical profile and can vary greatly from author to author. On the other hand, our fits of the total luminosity are good matches the the data ( $|m_{\text{model}} - m_{\text{observed}}| \sim 0.2 \text{ mags}$ ), and fall on the Tully-Fisher relation (Figure 8).

#### 4.4.6. Mass ratios

Figure 18 indicates that thick disk stars provide a significant fraction of a galaxy's total luminosity. However, as seen in Paper II, the thick disk tends to have a redder color than the thin disk, especially in low mass galaxies, and thus will have larger stellar mass-to-light ratios than the thin disk. Therefore, the thick disk may well dominate the stellar mass in many of our galaxies. We estimated the stellar disks' masses using the luminosities of the two disk components, along with color information from our single disk fits. Specifically we used the spectrophotometric galaxy evolution analysis of Bell & de Jong (2001) to convert our  $B - R$  color maps into stellar mass-to-light ratios for each disk, and then convert our luminosity ratios into mass ratios for the thick and thin components.

The initial analysis of vertical color gradients in our sample (Paper II) suggested that the colors of thin disks vary systematically with galaxy mass, but that the colors of thick disks are fairly uniform. We therefore assumed that the thick disks have uniform colors and mass-to-light ratios in each galaxy. To convert disk colors to masses, we first analyzed our  $R$ -band 2-disk fits to find regions where the thick disk contributes more than 75% of the total flux inside the  $1-\sigma$  noise contour. Out of 34 galaxies, 27 have a clearly thick disk dominated region. We created a model  $B - R$  color map of each galaxy using our 2-disk  $R$ -band model and single-disk  $B$ -band fits. Using the model images allowed us to avoid dust lanes, HII regions, and foreground objects that would complicate an analysis on the real images. We then used this color map to find the average  $B - R$  value in the thick disk dominated regions and took that as the approximate color for all the thick disk stars. We assumed the thick disk has a constant color, thereby guaranteeing that its structural parameters will be the same in both the  $B$  and  $R$  bands. With the  $B - R$  thick disk color from the model color map and the thick disk structural parameters from the 2-disk fit, we then made a model  $B - R$  color map for the thin disk by subtracting off the thick disk component from both the  $B$ -band and  $R$ -band models.

We applied internal extinction and reddening corrections to our models using the results of §4.3 and assumed

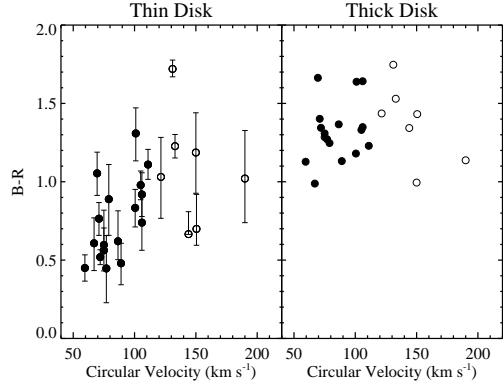


FIG. 20.— Extracted colors for the thick and thin disks. The thin disk colors shows the full range of  $B - R$  values for the midplane between  $h_R < R < 3h_R$ . The thin disk has been corrected for internal extinction, but we assume no correction for the thick disk. Open circles show galaxies with dust lanes.

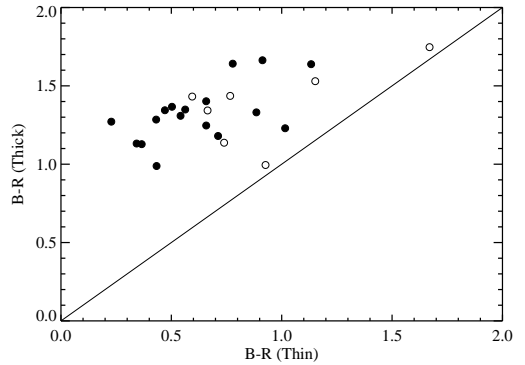


FIG. 21.— Comparison of thin and thick disk colors. The diagonal line indicates where the two components have equal color. Thin disk colors have been corrected for internal extinction. Open circles show galaxies with dust lanes.

that dust had a uniform effect on the thin disk colors but a negligible effect on the thick disk. Using this approximation, we found  $E(B - R) \sim 0.1$  for low mass galaxies and  $\sim 0.4$  for higher mass galaxies. Although it is only a rough approximation, our reddening correction is in good agreement with the radiative transfer model of Matthews & Wood (2001) who find that most disk light in their modeled edge-on galaxies suffer reddening of order  $E(B - R) \sim 0.1$ , and that the reddening saturates at  $E(B - R) = 0.31$ .

The resulting colors for thick and thin disks are plotted in Figure 20. The thick disks tend to be red with  $1.0 \lesssim B - R \lesssim 1.7$ , while the thin disks are blue in low mass galaxies and become nearly as red as the thick disks in the higher mass galaxies. This trend is also seen in Figure 21, where we directly compare the colors of each component.

Using the colors shown in Figure 20, and the color dependent stellar mass-to-light ratios from Bell & de Jong (2001), we converted the thick and thin disk luminosities to stellar masses using  $M = (M/L)_R L_R$ , where  $L_R$  is the extinction corrected  $R$ -band luminosity from §4.4.5. For the thin disk, we calculated  $(M/L)_R$  using the Bell & de Jong (2001) model which assumes a Salpeter

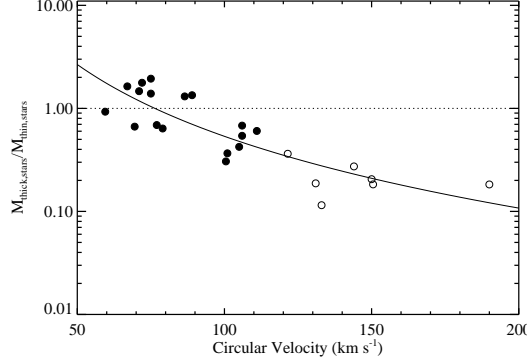


FIG. 22.— Stellar mass ratios of the thick and thin disks. The thin disks luminosities and corresponding masses have been increased to account for dust extinction. Galaxies with prominent dust lanes are plotted as open circles. The solid line is a power-law fit ( $M_{\text{thick}}/M_{\text{thin}})_{\text{stars}} = 0.53(V_c/100 \text{ km s}^{-1})^{-2.3}$ .

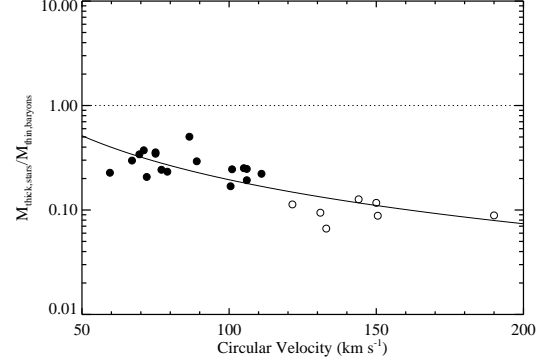


FIG. 23.— Baryonic mass ratios of the thick and thin disks. The thin disks luminosities, and corresponding masses, have been increased to account for extinction effects and include the estimated thin disk mass stored in gas. Galaxies with prominent dust lanes are plotted as open circles. The solid line is a power-law fit  $M_{\text{thick},\text{stars}}/M_{\text{thin},\text{baryons}} = 0.19(V_c/100 \text{ km s}^{-1})^{-1.4}$ .

IMF and metallicity of  $Z = 0.02$ , for the thick disk we use the same model with  $Z = 0.08$ . Overall, our results were insensitive to the stellar evolution and metallicity differences covered in the Bell & de Jong (2001) models.

The resulting mass ratios of the thick and thin disks are plotted in Figure 22. As expected, Figure 22 confirms the features from our luminosity analysis. First, there is a strong trend for lower mass galaxies to have a larger fraction of their stellar mass in a thick component. The trend has a Spearman correlation of  $\rho = -0.86$  ( $4.1\sigma$ ) and can be well fit with the relation  $M_{\text{thick}}/M_{\text{thin}} = 0.53(V_c/100 \text{ km s}^{-1})^{-2.3}$ . Second, in low mass galaxies,  $\sim 1/3$  to greater than  $1/2$  of the stellar mass is in the thick disk. Thus, the stellar mass of very low mass galaxies are dominated by thick disk stars.

Part of the trend in Figure 22 may be due to low star formation efficiency in lower mass disks. These systems have high gas mass fractions, and thus may not yet have built up a significant stellar mass in the thin disk. To investigate this possibility, we calculated the baryonic mass fraction of the thick and thin disks, assuming that all gas in the galaxies is associated with the thin disk and that the thick disk is entirely stellar. We calculate the gas mass as  $M_{\text{HI}}/M_{\odot} = 236d^2 \int S dV$  where  $d$  is the distance to the source in Mpc, and  $S$  is the flux density in mJy over the profile width  $dV$  in  $\text{km s}^{-1}$  (Zwaan et al. 1997). To account for He and metals, we make the standard correction  $M_{\text{gas}} = 1.4M_{\text{HI}}$ . We do not include a correction for molecular gas.

Figure 23 shows the resulting baryonic mass ratio of thick and thin disks with the mass of HI gas added to the thin disk component. When the gas is included in the thin disk component, we find that none of the galaxies remain thick disk dominated although the baryon mass fraction in the thick disk does remain substantial for low mass galaxies. Eleven of our galaxies had no HI data and their gas fraction was estimated by fitting a simple power law to the gas fraction of our galaxies with HI measurements. Figure 24 shows the final calculated baryon fractions for all of the stellar and gaseous components, and clearly indicates the increasing importance of the thick disk in lower mass galaxies.

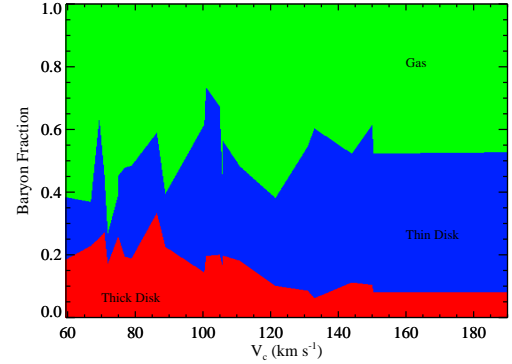


FIG. 24.— Final baryon fractions of the thick and thin components as a function of maximum velocity. The thin disk has been corrected for internal dust extinction. The baryonic mass fraction of the thick disk clearly increases towards lower galaxy mass.

## 5. THE FORMATION OF THE THICK DISK

Given evidence from the Milky Way and from nearby resolved galaxies, we will assume in the following discussion that thick disks have a formation mechanism distinct from that which forms the thin disk. We will also assume that the properties of “thick” and “thin” components from our 2-D fits will roughly approximate the properties of the chemically and kinematically distinct thick and thin disk analogs of the Milky Way. As we have argued above in §4.4.1, the structural properties of the fits are consistent with those of the corresponding components of the Milky Way and with the results of detailed stellar population studies in nearby galaxies (e.g. Figure 12). We therefore will simply assume a perfect correspondence between our fits and distinct thick and thin components for the rest of this discussion. While this assumption is not ideal, it is unavoidable, given that a full kinematic and chemical analysis of the stellar components is essentially impossible far outside the Local Group.

### 5.1. The Merger Origin of Thick Disks

As discussed above in §1, there are three general classes of thick disk formation scenarios – one where the thick disks stars form *in situ*, one where the thick disk stars form in a thin disk but are then impulsively “heated” to large scale heights, and one where thick disk stars form first in other galaxies but are then directly accreted. In the last decade there has been a growing body of evidence in favor of the latter two scenarios. This evidence includes the detection of strong kinematic differences between thick and thin disks in other galaxies (Yoachim & Dalcanton 2005) and in the Milky Way (Gilmore et al. 2002), as well as evidence from chemical abundance studies for extended star formation histories of Milky Way thick disk stars (e.g., Bensby et al. 2005). These latter two scenarios are also naturally accommodated in current theories of hierarchical structure formation, where mergers and accretion are common.

Of the two merger-driven scenarios, we believe that the data favor an accretion origin for thick disk stars. The strongest evidence comes from our previous measurements of thick and thin disk kinematics in two late-type disks. We found that thick disk stars are rotating with only a small fraction of the rotational velocity of thin disk stars, and are indeed counter-rotating in one of the two cases studied. In contrast to the observed behavior, simulations show that disks heated by satellites would have nearly the same angular momentum as the initial thin disk. Therefore, barring the unlikely possibility that the thin disk reforms from subsequent accretion of gas with angular momentum opposite to the original disk, creating counter-rotating or slowly-rotating thick disks via vertical heating alone is problematic. Additional supporting evidence comes from recent HST studies of resolved stars in nearby edge-on galaxies (Seth et al. 2005; Mould 2005). While Seth et al. (2005) finds evidence for some *steady* vertical heating, the oldest population of RGB stars shows no evidence of the vertical metallicity gradient expected if they were dominated by stars that had participated in the steady heating. Instead, the thick population of RGB stars must have been established early, when the merger rate was still extremely high. At these early times, the hypothetical picture of a well-defined stable thin disk impulsively heated by a single merging event seems inappropriate. In summary, while the evidence does not yet conclusively rule out a single, thin disk heating merger event as the origin of thick disk stars, we consider it to be sufficiently unlikely that we will focus on interpreting the results in this paper in terms of the accretion scenario.

The idea that stars well above the Galaxy’s midplane may have been directly accreted from satellites was first discussed by Statler (1988)<sup>4</sup>, and then codified as a distinct formation mechanism for the thick disk shortly thereafter in the review article by Gilmore et al. (1989) and as “Model 7” in Majewski (1993)’s review. Recent detailed studies of stellar structures in the Milky Way and M31 find evidence that stars are regularly accreted by massive galaxies. For example, Martin et al. (2004) find asymmetries in the distribution of M-giant

<sup>4</sup> Statler’s work refers to explaining the kinematics of “halo” stars, but given the current understanding of Galactic structure, the specific kinematic data he was trying to explain were measurements of what we would now call thick disk stars.

stars (e.g., the Galactic ‘Ring’ Newberg et al. 2002; Yanny et al. 2003) that are well explained by a single dwarf galaxy accretion event. Martin et al. (2004) also note that their modeled accretion event results in accreted stars having orbits similar to thick disk stars, and that the thick disk may be continually growing through in-plane accretion of dwarf galaxies. M31 also appears to also be actively disrupting dwarf galaxies with an observable stellar stream (Ibata et al. 2004) and a large extended disk (Ibata et al. 2005).

Direct accretion as the dominant origin of thick disk stars has recently been revived by several numerical studies of disk galaxy formation. Analyzing an N-body simulation of a moderately low mass spiral formed in a cosmological context, Abadi et al. (2003) found a well-populated thick disk, more than half of which was made up of stars originally formed in accreted satellite galaxies. Although by no means definitive due to the simulated galaxy’s unrealistically large bulge, Abadi et al. (2003)’s work lead to a revival of the notion that thick disk stars may have formed outside their host galaxies. Subsequent simulations of a collapsing sphere seeded with perturbations by Brook et al. (2004, 2005) generated thick disks associated with an early episode of chaotic merging. Unlike Abadi et al. (2003), Brook et al. (2004) argued that the thick disk stars formed *in situ* from large velocity dispersion gas deposited by the satellites as they merged together to the final disk structure. Both simulations have significant limitations, making it impossible to decide in favor of either scenario at this time, but both stress the importance of merging and accretion in setting properties of the thick disk.

In the context of hierarchical galaxy assembly, the above simulations point to a straightforward picture of disk formation that necessarily leads to the formation of thick disks. At high redshift, galaxies exist largely as a collection of sub-galactic fragments. These fragments consist of gravitationally bound dark matter “mini-halos”, many of which presumably host some amount of baryonic material. Because these systems are high in the merging hierarchy, they would be expected to be relatively dense, and thus some of the gas hosted by these sub-units is likely to form stars. Early on, the merging rate will be very high, and as these fragments come together, their orbits will tend to circularize, align, and decay due to dynamical friction, as in Statler (1988) and early simulations by Quinn & Goodman (1986) and Walker et al. (1996). The merged subunits will form a rotating flattened structure provided that the net angular momenta of the satellites is sufficiently high. When the merging rate declines sharply ( $z \sim 3$ ) (Zhao et al. 2003), the disk will be left in place as a long-lived structure relatively unperturbed by significant accretion events. Any dense gas associated with the pre-galactic fragments must then either form stars in a burst during the final merger of the fragments, as in the Brook et al. (2004) simulations, or cool into a thin disk which later converts into stars.

Within this scenario, *any* stars that formed in the sub-units and were not tidally stripped at large radii must necessarily wind up in a thickened disk structure, with a vertical velocity dispersion equal to or greater than the velocity dispersion of the typical pre-galactic fragment. Because they are effectively collisionless, the accreted

stars cannot lose energy and cool into a thinner disk, and must retain a large fraction of the initial velocity dispersion and angular momentum of the satellite in which they formed. With this in mind, it seems impossible to imagine *not* forming a thick disk (unless star formation was completely suppressed at early times, for example by reionization, e.g., Bullock et al. 2000; Gnedin 2000). The only other possible destination for the accreted stars would be the bulge or stellar halo. However, the sample considered here is essentially bulgeless. We also find no evidence for a luminous stellar halo down to our limiting surface brightness. Taking a conservative estimate for the surface brightness of the brightest stellar halo that could be present, but undetected in our data, we find that any stellar halo must be less than 15% of the luminosity of the thick disk. This estimate suggests that the majority of directly accreted stars settle into the thick disk.

In addition to the theoretical arguments for forming thick disks via direct accretion of stars, there is a slowly growing body of observational evidence for this process seen *in situ* at high redshift. First is the analysis of high redshift “clump-cluster” galaxies by Elmegreen & Elmegreen (2005). Morphologically, these galaxies appear to consist of many distinct, high surface brightness clumps merging together. Elmegreen & Elmegreen (2005) argue persuasively that these systems will wind up in a thickened disk with high velocity dispersion, and are thus likely precursors to thick disks. The colors of the clumps suggest that they already contain some stars, and are not pure gas systems. Elmegreen & Elmegreen (2005) also find field counterparts of the clumps, suggesting that some of the stars may have formed before being accreted into the galaxy. The second piece of evidence is the kinematic study of Erb et al. (2004), who find that lumpy disk-like structures at  $z \sim 2$  show little net rotation. If their sample consists primarily of the edge-on counterparts of the galaxies in the Elmegreen & Elmegreen (2005) study, then the lack of strong rotation would be consistent with what is expected for material that forms a thick disk. Although this study traces H $\alpha$  kinematics only, and thus leaves the kinematic state of any associated stars unconstrained, it would be peculiar if any stars associated with the accreting gas did not show similarly perturbed kinematics.

## 5.2. Constraints from the Structures of Thick and Thin Disks

In the above accretion scenario, the properties of the thick disk are fixed primarily by the stellar content and orbital properties of the pre-galactic fragments which merge to form the final stable disk. The properties of the thin and thick disks are then set by the kinematics and gas mass fractions of the pre-galactic fragments when they merge.

Within this scenario, we now discuss the implications of three significant properties of thick disks uncovered by our data: first, that thick disks are a ubiquitous and necessary component in modeling late-type edge-on galaxies; second, that the stellar mass of the thick disk is increasingly dominant in lower mass galaxies; and third, that thick disks have systematically larger radial scale lengths than thin disks.

### 5.2.1. The Ubiquity of Thick Disks

The 2-D fits of our sample confirm the initial suggestion of Dalcanton & Bernstein (2002) that thick disks are a ubiquitous component of disk galaxies. Essentially all (32 of 34) of the galaxies which were suitable for fitting were statistically significantly better fit by a second disk component (e.g. Figure 7). This result adds to the published detections of thick disks in earlier type systems (summarized in Table 2). Thick disks are now routinely discovered in every galaxy that has been searched for them<sup>5</sup>.

The evidence therefore supports the idea that thick disks are a generic property of all galaxies with disks, from S0's to Sm's, from high masses ( $V_c \sim 250 \text{ km s}^{-1}$ ) to low ( $V_c \sim 50 \text{ km s}^{-1}$ ). Thick disks must therefore be a natural by-product of disk galaxy formation, independent of the formation of a bulge. The ubiquity of thick disks can be easily explained if most thick disk stars are directly accreted from pre-galactic fragments. As we argue above, if *any* star formation has taken place in the fragments, some fraction of those stars must wind up in a thick disk. The only way to avoid depositing the stars in a thick disk would be if the fragments were completely tidally disrupted at large distances from the central galaxies. However, at large distances the matter density should be much lower than in the dense cores of the low mass galactic fragments, making it unlikely that every merging satellite would experience complete disruption.

The existence of widespread thick disks also suggests that there has been ample star formation in the very low mass halos which merge together to form larger galaxies. Most sub-units must have established stellar populations before merging. If instead the sub-units were entirely gaseous, disk galaxies would have only a thin disk component. Thus, there cannot have been total suppression of star formation by reionization up until the epoch of thick disk formation.

Finally, the pervasiveness of thick disks also presents an additional problem for merger heating scenarios. It seems unlikely that every galaxy in our sample would have had both a merger that created a thick disk and accretion that reformed a thin disk. If merger heating was the primary driver of thick disk formation we would expect to find some galaxies that were able to avoid a destructive merger, or that failed to subsequently reform a thin disk. Instead, all of our galaxies require both thin and thick disk components.

### 5.2.2. The Increasing Importance of Thick Disks in Lower Mass Galaxies

In the merging picture we have adopted, sub-galactic fragments contribute both stars and gas to the final galaxy. The stars wind up in the thick disk, and the gas settles into the thin disk, where it gradually converts

<sup>5</sup> The one exception is NGC 4244, which Fry et al. (1999) analyzed using fits to 1-D cuts of the vertical  $R$ -band light distribution. Based on the lack of a clear break in the vertical surface brightness profile, Fry et al. (1999) claimed there was no thick disk in this galaxy. However, subsequent analyses of the resolved stellar population in NGC 4244 by Seth et al. (2005) and Tikhonov et al. (2005) revealed the presence of a clear extra-planar population dominated by old red giant branch stars, whose global distribution was characteristic of a thick disk.

into stars. From Figure 24 we see that low mass disk galaxies have roughly 25% of their baryonic mass locked up into thick disk stars, while massive galaxies have only 10%. Figure 24 therefore implies a systematic variation in the gas richness of sub-galactic fragments at the time disks coalesce. In massive late-type galaxies, 90% of the baryonic mass must have remained gaseous during disk assembly, while in low mass galaxies only 75% had not yet converted to stars.

Note that while we are stressing the accretion of stellar material to form the thick disk, our results prove that the vast majority (75-90%) of baryonic accretion must have been gaseous. If some fraction of thick disk stars did form *in situ* as suggested by Brook, then the fraction of gaseous accretion must have been even higher.

There are several ways that lower gas mass fractions in the precursors of low mass galaxies may be achieved. One possibility is that the transformation of gas into stars proceeded further by the time the low mass disk galaxies coalesced. This more complete transformation in low mass disks could be due either to a later epoch of assembly, or to higher gas densities and thus higher star formation rates in the precursor clumps. However, in a closed box model, the resulting thick disk stars would have higher metallicities. In contrast, the estimates of the metallicities of extra-planar, RGB stars in Seth et al. (2005) suggest that the metallicities of the thick disk stars are systematically lower in lower mass galaxies, compared to the Milky Way. We therefore rule out the possibility that star formation was more “complete” in the precursors of lower mass galaxies.

Supernova feedback is an alternative pathway to the preponderance of less gas rich sub-units in low mass galaxies. Much of the disk material was initially in several subunits that were necessarily of lower mass than the final galaxy. Thus, the merging fragments must have had lower escape velocities, allowing supernova-driven winds to more effectively drive gas and metals from the galaxy at this early stage. The increased efficiency of SN winds in the sub-units would simultaneously decrease the gas mass fractions and maintain low metallicities in thick disk stars in low mass galaxies<sup>6</sup>.

We can estimate the amount of gas loss needed to produce the observed trends as follows. First, we assume that the observed baryon fraction in the stellar thin disk and gas component of massive galaxies ( $\sim 90\%$ , Figure 24) is indicative of the gas to stellar mass fraction in subgalactic fragments that are too massive to experience significant SN blowout. We then assume that the precursors of lower mass galaxies lose enough gas to bring their gas to stellar mass fraction down to  $\sim 75\%$  at the time of disk assembly. These simple assumptions imply that the sub-units of low mass galaxies must have lost 60% of their initial baryonic mass.

Because we have ignored possible tidal stripping of stars during galaxy assembly, the actual amount of gas

<sup>6</sup> Note, however, that the overall gas mass fraction of low mass galaxies can remain high to the present day. The disks of lower mass galaxies have systematically lower baryon surface densities (e.g., Swaters et al. 2002; Hunter & Elmegreen 2004), and thus are inefficient at converting gas into stars. Their low star formation rate thus allows them to have higher gas mass fractions today, even though they were comparatively gas poor at the time their disks were assembled.

lost from the precursors of low mass disks may be different from what we have estimated above. However, assuming that tidally stripped stars wind up in a stellar halo, we expect the total stellar mass lost to stripping to be small. The Milky Way’s thick disk contains a factor of  $\sim 10$  times more stars than its stellar halo, and thus, any correction due to tidal stripping is likely to be negligible.

While our mass-dependent blowout scenario explains our data well, it is not clear that pre-galactic fragments actually suffer  $\sim 60\%$  baryon losses due to SN winds. There are a wide range of results on how effective SN winds should be at driving baryon outflow. At the one extreme, several groups argue that large SN driven outflows exist in all galaxies with  $V_c < 100 \text{ km s}^{-1}$  (Dekel & Silk 1986; Dekel & Woo 2003). At the other extreme, simulations find that galaxies with  $M > 10^6 M_\odot$  experience almost no outflow (Mac Low & Ferrara 1999). Similarly, observational constraints on the extent of outflow vary. Mayer & Moore (2004) use the baryonic Tully-Fisher relation to claim that dwarf galaxies do not suffer large removal of baryons while Strickland et al. (2004) observe x-ray halos around massive star forming galaxies ( $M \sim 10^{10} - 10^{11} M_\odot$ ) which suggest they must have ejected at least some material. Because we are considering the role of blowout in low mass progenitors of our galaxy sample, we claim that the current knowledge of gas blowout is moderately consistent with our scenario and we await a more definitive cosmological simulation which incorporates star formation and feedback for detailed comparison to our model (Stinson et al., *in prep.*).

There are several limitations with the simplified analysis we have presented above. First, we have ignored the difficult question of how much material is accreted in continuous cold flows rather than bound in halos (Birnboim & Dekel 2003; Keres et al. 2004). Cold accretion of gas will tend to increase the baryonic fraction of the thin disk. Neglecting steady gas accretion therefore leads us to overestimate the gas richness of the merging pre-galactic fragments. Second, we have not explicitly considered how bulges are formed in the scenario discussed in §5.1, but we presume it involves repeated mergers of gas rich sub-units with little net angular momentum, or a higher frequency of major mergers in higher mass galaxies. Within the sample we have studies here, this omission is acceptable. However, more theoretical and observational work must be done to understand the thick disk population in earlier type galaxies.

Finally, we find it difficult to reconcile the Brook et al. (2004) formation scenario with the increasing fraction of thick disk stars in lower mass galaxies. Brook et al. (2004) suggest that thick disk stars form *in situ* from high velocity dispersion gas during the coalescence of sub-galactic fragments into a final disk. However, we see no obvious mechanism that could lead this scenario to produce a larger fraction of thick disk stars in low mass galaxies. One would need to invoke a mechanism to increase the efficiency of star formation at lower galaxy masses during mergers, while keeping star formation inefficient at later times. An alternative solution would be if steady cold flow gas accretion is more important in massive galaxies. However, massive galaxies are more likely to have established a hot shock-heated halo that would block cold flow (e.g., Dekel & Birnboim 2004). Thus,

the likely behavior of cold flow accretion has the opposite sign as what is needed to explain the high baryonic fraction of thick disks in low mass galaxies. Further simulations will help constrain this and other possible solutions.

### 5.2.3. The Scale Lengths of Thick & Thin Disks

Our data contribute to a growing number of observations finding that thick disks have larger scale lengths than their embedded thin disks (Ojha 2001; Larsen & Humphreys 2003; Wu et al. 2002; Pohlen et al. 2004, see our Figure 13, and Table 2). The large scale lengths of thick disks argue against their being formed via vertical heating of a thin disk. N-body simulations find that while minor mergers can vertically heat a disk, they do not increase its scale length (Quinn et al. 1993). Such mergers also tend to leave the galaxy looking like an earlier Hubble type (Walker et al. 1996) while all of our galaxies have no prominent bulge components. As an example, simulations by Aguerri et al. (2001) find that minor mergers can extend the scale length of the thin disk somewhat, by 10-60%. However, the same simulations also produce a large bulge, which is incompatible with our sample.

In contrast, in the accretion scenario one would expect the scale length of the thin disk to be somewhat smaller than that of the thick disk. If the thin disk forms later from gas which has contracted further into halo than the thick disk stars, it should have a smaller scale length. If angular momentum is largely conserved, then the thin disk should also be rotating somewhat faster than the thick disk because of its extra contraction.

The satellite accretion model therefore suggests that there may be correlations between the radial scale lengths and the kinematics of the thick and thin disks. Results in Section 4.4.2 and photometric decompositions by others (Ojha 2001; Larsen & Humphreys 2003; Wu et al. 2002; Pohlen et al. 2004) suggest that scale lengths of thick disks are roughly 30% longer than those of their embedded thin disks, on average. Simple angular momentum conservation would then suggest that the thick disk should rotate with approximately 2/3 the speed of the thin disk, in rough agreement with the Milky Way and FGC 1415 (Yoachim & Dalcanton 2005). However, the inclusion of any counter-rotating material in the merger could easily break this correlation. For example, the kinematics of FGC 227 indicate that the satellites which contributed the majority of the baryons to the thin disk could not also have deposited the majority of the thick disk stars. This particular formation pathway allows the scale lengths of the thick and thin disks to sometimes decouple, and indeed, the scale lengths of FGC 227's thick disk is comparable to, not larger than, its thin disk.

The structural parameters of the thick disks formed in the Abadi et al. (2003) and Brook et al. (2004, 2005) simulations are in moderate agreement with our results. However, direct comparisons are difficult because the simulated galaxies tend to be more massive than the galaxies in our sample and also host large bulge components. The simulated thick disks do seem to match the observed trends of scale height ratios (Figure 11) and luminosity ratios (Figure 19). However, the scale length ratio found in the Brook et al. (2005) simulation is fairly

low (Figure 15), possibly due to the fact that their thick disk stars are formed directly from the gas during mergers, increasing the likelihood that the thick and thin disk stars will share similar scale lengths and kinematics. It is also difficult to compare our 2-d decompositions with analysis of simulations that can separate stellar populations based on kinematics.

## 5.3. Further Implications

Given the excellent fit to the body of data on thick disks, we now begin to address other implications of the accretion scenario developed above.

### 5.3.1. Old Low Mass Galaxies

In hierarchical galaxy formation models, small scale structure collapses first, suggesting that low mass galaxies should be old. This expectation is in direct conflict with observations that low mass galaxies almost always have blue colors consistent with young stellar populations. This difference is one of the most intractable failings of the predictions of semi-analytic models (e.g. Bell et al. 2003; van den Bosch 2002). The existence of thick disks that dominate the stellar mass of low mass galaxies (Figure 22) solves this conundrum. Our observations show that low mass galaxies are indeed *dominated* by an old stellar population, but one that is sufficiently old, faint, and diffuse that it has no significant impact on the observed colors of the young, high-surface brightness, star-forming thin disk (§4.4.4). We believe that semi-analytic models could be brought into alignment with the data if they were to include both the locking up of material into a diffuse thick disk and the suppression of star formation efficiencies in low mass disks due to their lying entirely below the Kennicutt star formation threshold (e.g., Verde et al. 2002; Dalcanton et al. 2004).

### 5.3.2. Abundance patterns and the timing of thick and thin disk formation

Studies of  $\alpha$ -element abundances of the Milky Way have suggested that star formation in the thick disk took place over several gigayears (e.g., Bensby et al. 2004a). The abundances in thick disk stars show a flat plateau at high  $[\alpha/\text{Fe}]$  that extends to  $[\text{Fe}/\text{H}] \sim -0.3$ , indicating that thick disk stars enriched quickly to relatively high metallicity, before Type Ia supernovae became prevalent. At larger iron abundances ( $-0.3 < [\text{Fe}/\text{H}] \lesssim 0$ ), however, the  $\alpha$  abundance declines linearly, suggesting that star formation in the thick disk was sufficiently extended ( $\gtrsim 1 - 3$  Gyr) that enrichment from Type Ia's became important. The abundances of thin disk stars show similar, parallel behavior, but the plateau does not extend to equally high metallicities, indicating that early star formation in the thin disk was not nearly as rapid as in the thick disk. The abundance patterns of thick and thin disk stars therefore follow parallel but distinct sequences on the  $[\alpha/\text{Fe}]$  vs  $[\text{Fe}/\text{H}]$  plane, with significant overlap in  $[\text{Fe}/\text{H}]$  (most recently Bensby et al. 2004b; Mishenina et al. 2004; Gratton et al. 2003).

The above sequence of events is typically taken as evidence that the thick disk formed from violent heating of a previous thinner disk. However, it may be possible to accommodate the abundance data in the accretion scenario as well. First, the rapid enrichment of future thick

disk stars can easily occur in the pre-galactic fragments. These mini-halos should be dense, leading to high gas densities and star formation rates, which would produce the necessary fast enrichment. While we have hypothesized above that supernova-driven winds will truncate star formation in the lower mass progenitors, some mini-halos will have sufficient mass to retain gas for longer periods of time, allowing stars to form over sufficiently long timescales to produce both the drop in  $[\alpha/\text{Fe}]$  and the enrichment of some thick disk stars to near solar metallicities.

The expected timescales for this scenario are compatible with the observational constraints. Theory suggests that the epoch of thick disk assembly should correspond to the period of rapid mass accretion seen in simulations at  $z \gtrsim 3$ , or  $t_{\text{lookback}} \gtrsim 11$  Gyr (e.g., Zhao et al. 2003). Observationally, the relative abundance of  $[\text{Eu}/\text{Ba}]$  indicates that thick disk stars were formed on a timescale of 1-1.5 Gyr (Mashonkina et al. 2003), which makes the theoretical expectation consistent with the age of the universe determined from WMAP.

In addition to the short star formation timescale for thick disk stars, the accretion scenario can produce a long timescale for formation of thin disk stars. After the pre-galactic fragments merge into a disk, the gas that forms the thin disk gradually converts into stars. The timescale of this conversion is controlled primarily by the gas surface density. In general, this timescale should be much longer in the disk than in the pre-galactic fragments, because the gas is spread over much larger areas, leading to lower gas densities and longer star formation timescales. The difference in timescales for thick and thin disk star formation could lead to the appearance of a “delay” between the formation of the two components. However, as accretion of both gas and stars would be ongoing from early times until  $z \sim 3$ , some genuinely old thick disk stars would be allowed to form (see discussion in Abadi et al. 2003).

The accretion scenario also provides a mechanism for producing thin disk stars with lower  $\alpha$ -abundances than thick disk stars at the same metallicity. Because the thin disk assembles from gas that had not been consumed by star formation in pre-galactic fragments, it is possible for the gas to initially have lower mean metallicity than the thick disk stars that were accreted. The gas may come from larger radii within individual mini-halos, and thus be less enriched. It may also come from fragments that have never formed stars, or from cold flow accretion directly. Thus, accretion may allow the youngest thin disk stars to be sufficiently metal-poor that they overlap the metallicities of thick disk stars.

The one significant trouble spot is the thinness of the observed  $[\alpha/\text{Fe}]$  vs  $[\text{Fe}/\text{H}]$  relation for thick disk stars. If the thick disk formed from assembly of many different sub-units of different masses, lifetimes, and gas richesses, then one might expect large variations in the degree of  $\alpha$ -enhancement in the accreted stars. On the other hand, the potential discrepancy might not be as severe as one might initially believe. If supernova-driven winds truncate star formation in low mass sub-units, then only the most massive mini-halos contribute stars to the high metallicity ( $[\text{Fe}/\text{H}] \gtrsim -0.3$ ) thick disk, since they are the only precursors that could hold gas long enough to allow significant Type Ia enrichment. Massive halos

are rarer than low mass halos, and thus a relatively small number of halos may dominate the metal rich end of the thick disk population, much in the way that  $L_*$  galaxies dominate the luminosity density of the local universe. These disrupted satellites may also segregate to different radii, as seen in the Abadi et al. (2003) simulations, such that a sample at the solar circle is dominated by an even smaller number of massive satellites. More detailed simulations are needed to evaluate the size of this possible discrepancy.

### 5.3.3. Pre-Enrichment of Thin Disks

Chemical abundance data on stars within the Milky Way has led to the conclusion that the thin disk may have been “pre-enriched” (e.g., Caimmi 2000; Chiappini et al. 1997; Pagel & Tautvaisiene 1995). Such pre-enrichment naturally explains the lack of truly metal poor stars in the thin disk as well as the under-abundance of more moderately metal-poor stars (i.e. the “G-Dwarf” problem). In the scenario we have explored here, the gas from which thin disk stars form was originally associated with the thick disk, and thus will have been enriched while still in pre-galactic fragments. While this idea has been suggested before (e.g., Brook et al. 2005), the universality of thick disks suggests that it is probably a wide-spread, phenomena.

### 5.3.4. Producing the Mass-Metallicity Relationship in Disks

Another attractive feature of the satellite accretion model is that it facilitates creating the mass-metallicity relationship in disks. Many authors have argued that the lower metallicities and effective yields seen in low mass galaxies is due to the onset of supernova-driven winds at the mass scale where the metallicity begins to fall ( $V_c \sim 120 \text{ km s}^{-1}$ , or  $M_{\text{baryon}} < 3 \times 10^{10} M_\odot$ ; e.g. Garnett 2002; Tremonti et al. 2004; Dekel & Woo 2003; Kauffmann et al. 2003). However, simulations of gas outflow find that it is quite difficult to drive coherent winds at these masses (Ferrara & Tolstoy 2000), particularly given the low star formation rates typical of low mass disks (e.g. Hunter & Elmegreen 2004).

As an alternative, the satellite accretion model suggests that non-negligible star formation took place in lower mass sub-units. These pre-galactic fragments had much lower escape velocities, and probably had higher gas surface densities due to not yet being organized into a coherent rotating disk. Thus, the sub-units are a more natural environment for driving winds, given their low escape velocities and likely high star formation rates. The origin of the observed mass-metallicity relation may therefore lie not so much in the disks themselves, but in the sub-units from which they assembled.

## 6. CONCLUSIONS

We fit thin and thick disk components to a sample of 34 late-type edge-on spiral galaxies. Our thick disk components are very similar to previously detected thick disk systems and the MW thick disk, suggesting they are a remnant stellar population left over from early stages of galaxy formation. In lower mass galaxies ( $V_c < 100 \text{ km s}^{-1}$ ), the thick disk is the dominant component in both luminosity and stellar mass. For higher mass galaxies,

the thick disk is a minor component, and is analogous to the thick disks found in the Milky Way and other higher mass galaxies. In particular, we find:

- Thick disks have a scale height  $\sim 2$  times larger than thin disks
- Thick disks have systematically larger scale lengths than thin disks
- In low mass galaxies, the thick disk can dominate the total  $R$ -band luminosity
- The thick disk comprises 5-40% of the total baryonic mass of our galaxies

We combine these results with the findings of other studies of thick disks to analyze possible thick disk formation scenarios. In particular, we include results from thick disk kinematics (Yoachim & Dalcanton 2005), studies of resolved stellar populations in thick disks (Seth et al. 2005; Mould 2005), and simulations which form thick disks (Brook et al. 2004; Brook et al. 2005; Abadi et al. 2003). Overall, we find that models where the thick disk forms from a kinematically heated thin disk is not supported by the data. Instead, our results favor models where thick disk stars formed in galactic sub-units before merging to create the final galaxy.

We consider a hierarchical galaxy formation scenario where galaxies form through a series of mergers where sub-units deposit both stars and gas. Any stellar component in the sub-units end up in the thick disk, while gas cools and forms a thin disk. We find that the low mass galaxies in our sample must have formed from sub-units that had a higher stellar mass fraction than those that formed higher mass galaxies. We can explain this result if low mass sub-units (which go on to form low mass galaxies) are more susceptible to SN-induced blowout, leaving them with a higher stellar to gas mass fraction. A mass-dependent blowout scenario is consistent with other general observations of disk galaxies, such as the mass-metallicity relation and the chemical pre-enrichment of the MW thin disk.

Thanks to Greg Stinson, Anil Seth, and Alyson Brooks for stimulating conversations. JJD and PY were partially supported through NSF grant CAREER AST-0238683 and the Alfred P. Sloan Foundation. This research made extensive use of distributed computing with Condor software: The Condor Software Program (Condor) was developed by the Condor Team at the Computer Sciences Department of the University of Wisconsin-Madison. All rights, title, and interest in Condor are owned by the Condor Team.

## REFERENCES

Abadi, M. G., Navarro, J. F., Steinmetz, M., & Eke, V. R. 2003, *ApJ*, 597, 21

Abe, F., Bond, I. A., Carter, B. S., Dodd, R. J., Fujimoto, M., Hearnshaw, J. B., Honda, M., Jugaku, J., Kabe, S., Kilmartin, P. M., Koribalski, B. S., Kobayashi, M., Masuda, K., Matsubara, Y., Miyamoto, M., Muraki, Y., Nakamura, T., Nankivell, G. R., Noda, S., Pennycook, G. S., Pipe, L. Z., Rattenbury, N. J., Reid, M., Rumsey, N. J., Saito, T., Sato, H., Sato, S., Sekiguchi, M., Sullivan, D. J., Sumi, T., Watase, Y., Yanagisawa, T., Yock, P. C. M., & Yoshizawa, M. 1999, *AJ*, 118, 261

Aguerri, J. A. L., Balcells, M., & Peletier, R. F. 2001, *A&A*, 367, 428

Bahcall, J. N., & Soneira, R. M. 1980, *ApJS*, 44, 73

Barton, I. J., & Thompson, L. A. 1997, *AJ*, 114, 655

Begum, A., Chengalur, J. N., & Karachentsev, I. D. 2005, *A&A*, 433, L1

Bell, E. F., Baugh, C. M., Cole, S., Frenk, C. S., & Lacey, C. G. 2003, *MNRAS*, 343, 367

Bell, E. F., & de Jong, R. S. 2001, *ApJ*, 550, 212

Bensby, T., Feltzing, S., & Lundström, I. 2003, *A&A*, 410, 527

—. 2004a, *A&A*, 421, 969

—. 2004b, *A&A*, 415, 155

Bensby, T., Feltzing, S., Lundström, I., & Ilyin, I. 2005, *A&A*, 433, 185

Binggeli, B., & Popescu, C. C. 1995, *A&A*, 298, 63

Birnboim, Y., & Dekel, A. 2003, *MNRAS*, 345, 349

Bizyaev, D., & Mitronova, S. 2002, *A&A*, 389, 795

Brewer, M., & Carney, B. W. 2004, *Publications of the Astronomical Society of Australia*, 21, 134

Brook, C. B., Gibson, B. K., Martel, H., & Kawata, D. 2005, *astro-ph/0503273*

Brook, C. B., Kawata, D., Gibson, B. K., & Flynn, C. 2003, *ApJ*, 585, L125

Brook, C. B., Kawata, D., Gibson, B. K., & Freeman, K. C. 2004, *ApJ*, 612, 894

Bruzual, G., & Charlot, S. 2003, *MNRAS*, 344, 1000

Bullock, J. S., Kravtsov, A. V., & Weinberg, D. H. 2000, *ApJ*, 539, 517

Burkert, A., Truran, J. W., & Hensler, G. 1992, *ApJ*, 391, 651

Burstein, D. 1979, *ApJ*, 234, 829

Buser, R., Rong, J., & Karaali, S. 1999, *A&A*, 348, 98

Caimmi, R. 2000, *Astronomische Nachrichten*, 321, 323

Chen, B., Stoughton, C., Smith, J. A., Uomoto, A., Pier, J. R., Yanny, B., Ivezic, Z., York, D. G., Anderson, J. E., Annis, J., Brinkmann, J., Csabai, I., Fukugita, M., Hindsley, R., Lupton, R., Munn, J. A., & the SDSS Collaboration. 2001, *ApJ*, 553, 184

Chiappini, C., Matteucci, F., & Gratton, R. 1997, *ApJ*, 477, 765

Chiba, M., & Beers, T. C. 2000, *AJ*, 119, 2843

Dalcanton, J. J., & Bernstein, R. A. 2000, *AJ*, 120, 203

—. 2002, *AJ*, 124, 1328

Dalcanton, J. J., Yoachim, P., & Bernstein, R. A. 2004, *ApJ*, 608, 189

de Grijs, R., & Peletier, R. F. 1997, *A&A*, 320, L21

de Grijs, R., Peletier, R. F., & van der Kruit, P. C. 1997, *A&A*, 327, 966

de Grijs, R., & van der Kruit, P. C. 1996, *A&AS*, 117, 19

de Jong, R. S. 1996, *A&AS*, 118, 557

Dekel, A., & Birnboim, Y. 2004, *astro-ph/0412300*

Dekel, A., & Silk, J. 1986, *ApJ*, 303, 39

Dekel, A., & Woo, J. 2003, *MNRAS*, 344, 1131

Dove, J. B., & Thronson, H. A. 1993, *ApJ*, 411, 632

Eggen, O. J., Lynden-Bell, D., & Sandage, A. R. 1962, *ApJ*, 136, 748

Elmegreen, B. G., & Elmegreen, D. M. 2005, *ApJ*, 627, 632

Erb, D. K., Steidel, C. C., Shapley, A. E., Pettini, M., & Adelberger, K. L. 2004, *ApJ*, 612, 122

Feltzing, S., Bensby, T., Gesse, S., & Lundström, I. 2004, in *Origin and Evolution of the Elements*

Feltzing, S., Bensby, T., & Lundström, I. 2003, *A&A*, 397, L1

Ferrara, A., & Tolstoy, E. 2000, *MNRAS*, 313, 291

Freeman, K. C. 1970, *ApJ*, 160, 811

Fry, A. M., Morrison, H. L., Harding, P., & Boroson, T. A. 1999, *AJ*, 118, 1209

Fuhrmann, K. 1998, *A&A*, 338, 161

—. 2004, *Astronomische Nachrichten*, 325, 3

Garnett, D. R. 2002, *ApJ*, 581, 1019

Gilmore, G., & Reid, N. 1983, *MNRAS*, 202, 1025

Gilmore, G., & Wyse, R. F. G. 1986, *Nature*, 322, 806

Gilmore, G., Wyse, R. F. G., & Kuijken, K. 1989, *ARA&A*, 27, 555

Gilmore, G., Wyse, R. F. G., & Norris, J. E. 2002, *ApJ*, 574, L39

Gnedin, N. Y. 2000, *ApJ*, 542, 535

Gratton, R. G., Carretta, E., Desidera, S., Lucatello, S., Mazzei, P., & Barbieri, M. 2003, *A&A*, 406, 131

Guhathakurta, P., et al. 2005, *astro-ph/0502366*

Hodge, P. W., & Hitchcock, J. L. 1966, PASP, 78, 79

Hunter, D. A., & Elmegreen, B. G. 2004, AJ, 128, 2170

Ibata, R., Chapman, S., Ferguson, A. M. N., Irwin, M., Lewis, G., & McConnachie, A. 2004, MNRAS, 351, 117

Ibata, R., et al. 2005, astro-ph/0504164

Karachentsev, I. D., Karachentseva, V. E., Kudrya, Y. N., Makarov, D. I., & Parnovskiy, S. L. 2000, Bull. Special Astrophys. Obs., 50, 5

Karachentsev, I. D., Karachentseva, V. E., & Parnovskij, S. L. 1993, Astronomische Nachrichten, 314, 97

Kauffmann, G., Heckman, T. M., White, S. D. M., Charlot, S., Tremonti, C., Peng, E. W., Seibert, M., Brinkmann, J., Nichol, R. C., SubbaRao, M., & York, D. 2003, MNRAS, 341, 54

Keres, D., Katz, N., Weinberg, D. H., & Dave, R. 2004, astro-ph/0407095

Kregel, M., & van der Kruit, P. C. 2004, MNRAS, 355, 143

Kregel, M., van der Kruit, P. C., & de Grijs, R. 2002, MNRAS, 334, 646

Kroupa, P. 2002, MNRAS, 330, 707

Kudrya, Y. N., Karachentsev, I. D., Karachentseva, V. E., & Parnovskij, S. L. 1994, Astronomy Letters, 20, 8

Larsen, J. A., & Humphreys, R. M. 2003, AJ, 125, 1958

Mac Low, M., & Ferrara, A. 1999, ApJ, 513, 142

MacArthur, L. A., Courteau, S., Bell, E., & Holtzman, J. A. 2004, ApJS, 152, 175

MacArthur, L. A., Courteau, S., & Holtzman, J. A. 2003, ApJ, 582, 689

Majewski, S. R. 1993, ARA&A, 31, 575

Martin, N. F., Ibata, R. A., Bellazzini, M., Irwin, M. J., Lewis, G. F., & Dehnen, W. 2004, MNRAS, 348, 12

Mashonkina, L., Gehren, T., Travaglio, C., & Borkova, T. 2003, A&A, 397, 275

Matthews, L. D. 2000, AJ, 120, 1764

Matthews, L. D., & Wood, K. 2001, ApJ, 548, 150

Mayer, L., & Moore, B. 2004, MNRAS, 354, 477

Mishenina, T. V., Soubiran, C., Kovtyukh, V. V., & Korotin, S. A. 2004, A&A, 418, 551

Morrison, H. L., Miller, E. D., Harding, P., Stinebring, D. R., & Boroson, T. A. 1997, AJ, 113, 2061

Mould, J. 2005, AJ, 129, 698

Neeser, M. J., Sackett, P. D., De Marchi, G., & Paresce, F. 2002, A&A, 383, 472

Newberg, H. J., Yanny, B., Rockosi, C., Grebel, E. K., Rix, H., Brinkmann, J., Csabai, I., Hennessy, G., Hindsley, R. B., Ibata, R., Ivezic, Z., Lamb, D., Nash, E. T., Odenkirchen, M., Rave, H. A., Schneider, D. P., Smith, J. A., Stolte, A., & York, D. G. 2002, ApJ, 569, 245

Nissen, P. E. 1995, in IAU Symp. 164: Stellar Populations, 109–+

Norris, J. E. 1999, Ap&SS, 265, 213

Norris, J. E., & Ryan, S. G. 1991, ApJ, 380, 403

Ojha, D. K. 2001, MNRAS, 322, 426

Pagel, B. E. J., & Tautvaišienė, G. 1995, MNRAS, 276, 505

Parker, J. E., Humphreys, R. M., & Beers, T. C. 2004, AJ, 127, 1567

Pohlen, M., Balcells, M., Lüticke, R., & Dettmar, R.-J. 2004, A&A, 422, 465

Pohlen, M., Dettmar, R.-J., & Lüticke, R. 2000, A&A, 357, L1

Pohlen, M., Dettmar, R.-J., Lüticke, R., & Aronica, G. 2002, A&A, 392, 807

Prochaska, J. X., Naumov, S. O., Carney, B. W., McWilliam, A., & Wolfe, A. M. 2000, AJ, 120, 2513

Quinn, P. J., & Goodman, J. 1986, ApJ, 309, 472

Quinn, P. J., Hernquist, L., & Fullagar, D. P. 1993, ApJ, 403, 74

Reid, N., & Majewski, S. R. 1993, ApJ, 409, 635

Robin, A. C., Haywood, M., Creze, M., Ojha, D. K., & Bienaymé, O. 1996, A&A, 305, 125

Sakai, S., Mould, J. R., Hughes, S. M. G., Huchra, J. P., Macri, L. M., Kennicutt, R. C., Gibson, B. K., Ferrarese, L., Freedman, W. L., Han, M., Ford, H. C., Graham, J. A., Illingworth, G. D., Kelson, D. D., Madore, B. F., Sebo, K., Silbermann, N. A., & Stetson, P. B. 2000, ApJ, 529, 698

Seth, A. C., Dalcanton, J. J., & de Jong, R. S. 2005, AJ, 129, 1331

Seth, A. C., Dalcanton, J. J., & De Jong, R. S. 2005, astro-ph/0506117

Shaw, M. A., & Gilmore, G. 1990, MNRAS, 242, 59

Soubiran, C., Bienaymé, O., & Siebert, A. 2003, A&A, 398, 141

Spitzer, L. J. 1942, ApJ, 95, 329

Statler, T. S. 1988, ApJ, 331, 71

Staveley-Smith, L., Davies, R. D., & Kinman, T. D. 1992, MNRAS, 258, 334

Strickland, D. K., Heckman, T. M., Colbert, E. J. M., Hoopes, C. G., & Weaver, K. A. 2004, ApJ, 606, 829

Sung, E., Han, C., Ryden, B. S., Patterson, R. J., Chun, M., Kim, H., Lee, W., & Kim, D. 1998, ApJ, 505, 199

Swaters, R. A., & Balcells, M. 2002, A&A, 390, 863

Swaters, R. A., van Albada, T. S., van der Hulst, J. M., & Sancisi, R. 2002, A&A, 390, 829

Tautvaišienė, G., Edvardsson, B., Tuominen, I., & Ilyin, I. 2001, A&A, 380, 578

Tikhonov, N. A., Galazutdinova, O. A., & Drozdovsky, I. O. 2005, A&A, 431, 127

Tremonti, C. A., Heckman, T. M., Kauffmann, G., Brinchmann, J., Charlot, S., White, S. D. M., Seibert, M., Peng, E. W., Schlegel, D. J., Uomoto, A., Fukugita, M., & Brinkmann, J. 2004, ApJ, 613, 898

Tsikoudi, V. 1979, ApJ, 234, 842

Tully, R. B., Pierce, M. J., Huang, J., Saunders, W., Verheijen, M. A. W., & Witchalls, P. L. 1998, AJ, 115, 2264

van den Bosch, F. C. 2002, MNRAS, 332, 456

van der Kruit, P. C. 1988, A&A, 192, 117

van der Kruit, P. C., & Searle, L. 1981a, A&A, 95, 116

—. 1981b, A&A, 95, 105

—. 1982, A&A, 110, 61

van Dokkum, P. G., Peletier, R. F., de Grijs, R., & Balcells, M. 1994, A&A, 286, 415

Velazquez, H., & White, S. D. M. 1999, MNRAS, 304, 254

Verde, L., Oh, S. P., & Jimenez, R. 2002, MNRAS, 336, 541

Verheijen, M. A. W. 2001, ApJ, 563, 694

Wainscoat, R. J., Freeman, K. C., & Hyland, A. R. 1989, ApJ, 337, 163

Walker, I. R., Mihos, J. C., & Hernquist, L. 1996, ApJ, 460, 121

Weiner, B. J., Williams, T. B., van Gorkom, J. H., & Sellwood, J. A. 2001, ApJ, 546, 916

Wu, H., Burstein, D., Deng, Z., Zhou, X., Shang, Z., Zheng, Z., Chen, J., Su, H., Windhorst, R. A., Chen, W., Zou, Z., Xia, X., Jiang, Z., Ma, J., Xue, S., Zhu, J., Cheng, F., Byun, Y., Chen, R., Deng, L., Fan, X., Fang, L., Kong, X., Li, Y., Lin, W., Lu, P., Sun, W., Tsay, W., Xu, W., Yan, H., Zhao, B., & Zheng, Z. 2002, AJ, 123, 1364

Yahil, A., Tammann, G. A., & Sandage, A. 1977, ApJ, 217, 903

Yanny, B., Newberg, H. J., Grebel, E. K., Kent, S., Odenkirchen, M., Rockosi, C. M., Schlegel, D., Subbarao, M., Brinkmann, J., Fukugita, M., Ivezic, Z., Lamb, D. Q., Schneider, D. P., & York, D. G. 2003, ApJ, 588, 824

Yoachim, P., & Dalcanton, J. J. 2005, ApJ, 624, 701

Zhao, D. H., Jing, Y. P., Mo, H. J., & Börner, G. 2003, ApJ, 597, L9

Zibetti, S., White, S. D. M., & Brinkmann, J. 2004, MNRAS, 347, 556

Zwaan, M. A., Briggs, F. H., Sprayberry, D., & Sorar, E. 1997, ApJ, 490, 173

TABLE 3  
SINGLE DISK FITS FOR THE SAMPLE GALAXIES.

FGC	Adopted Distance <sup>1</sup> Mpc	B			R			K <sub>s</sub>		
		$\mu(0,0)$ (mag/ $\square''$ )	$h_r$ ( $''$ )	$z_0$ ( $''$ )	$\mu(0,0)$ (mag/ $\square''$ )	$h_r$ ( $''$ )	$z_0$ ( $''$ )	$\mu(0,0)$ (mag/ $\square''$ )	$h_r$ ( $''$ )	$z_0$ ( $''$ )
31	51.9	22.67 <sub>-0.01</sub> <sup>+0.01</sup>	10.1 <sub>-0.61</sub> <sup>+0.62</sup>	1.96 <sub>-0.10</sub> <sup>+0.05</sup>	21.93 <sub>-0.07</sub> <sup>+0.03</sup>	8.9 <sub>-0.20</sub> <sup>+0.05</sup>	2.06 <sub>-0.13</sub> <sup>+0.05</sup>	20.01 <sub>-0.19</sub> <sup>+0.01</sup>	6.91 <sub>-0.00</sub> <sup>+1.35</sup>	1.95 <sub>-0.05</sub> <sup>+0.21</sup>
36	80.9	22.33 <sub>-0.09</sub> <sup>+0.03</sup>	8.5 <sub>-0.37</sub> <sup>+1.10</sup>	1.71 <sub>-0.04</sub> <sup>+0.07</sup>	21.06 <sub>-0.12</sub> <sup>+0.04</sup>	7.4 <sub>-0.41</sub> <sup>+0.74</sup>	1.73 <sub>-0.08</sub> <sup>+0.12</sup>	18.51 <sub>-0.02</sub> <sup>+0.15</sup>	6.80 <sub>-0.06</sub> <sup>+0.93</sup>	1.64 <sub>-0.06</sub> <sup>+0.08</sup>
130	233.1	22.67 <sub>-0.03</sub> <sup>+0.09</sup>	9.4 <sub>-0.12</sub> <sup>+1.95</sup>	1.63 <sub>-0.00</sub> <sup>+0.04</sup>	21.15 <sub>-0.10</sub> <sup>+0.00</sup>	8.4 <sub>-0.07</sub> <sup>+0.61</sup>	1.71 <sub>-0.04</sub> <sup>+0.07</sup>	17.17 <sub>-0.16</sub> <sup>+0.01</sup>	6.50 <sub>-0.19</sub> <sup>+0.50</sup>	1.27 <sub>-0.06</sub> <sup>+0.05</sup>
164	69.9	22.88 <sub>-0.03</sub> <sup>+0.07</sup>	10.7 <sub>-0.28</sub> <sup>+0.57</sup>	1.63 <sub>-0.12</sub> <sup>+0.30</sup>	22.24 <sub>-0.07</sub> <sup>+0.04</sup>	9.8 <sub>-0.17</sub> <sup>+0.61</sup>	1.86 <sub>-0.16</sub> <sup>+0.32</sup>	20.38 <sub>-0.02</sub> <sup>+0.01</sup>	8.60 <sub>-0.31</sub> <sup>+0.42</sup>	1.87 <sub>-0.07</sub> <sup>+0.02</sup>
215	131.1	22.46 <sub>-0.01</sub> <sup>+0.08</sup>	12.8 <sub>-0.33</sub> <sup>+1.81</sup>	1.71 <sub>-0.02</sub> <sup>+0.04</sup>	21.21 <sub>-0.16</sub> <sup>+0.04</sup>	11.4 <sub>-0.63</sub> <sup>+0.52</sup>	1.64 <sub>-0.08</sub> <sup>+0.11</sup>	17.93 <sub>-0.12</sub> <sup>+0.10</sup>	7.41 <sub>-0.91</sub> <sup>+1.36</sup>	1.23 <sub>-0.03</sub> <sup>+0.01</sup>
225	74.3	22.29 <sub>-0.05</sub> <sup>+0.02</sup>	8.9 <sub>-0.72</sub> <sup>+0.24</sup>	2.41 <sub>-0.07</sub> <sup>+0.02</sup>	21.31 <sub>-0.11</sub> <sup>+0.02</sup>	8.2 <sub>-0.61</sub> <sup>+0.05</sup>	2.40 <sub>-0.12</sub> <sup>+0.07</sup>	19.28 <sub>-0.18</sub> <sup>+0.02</sup>	7.71 <sub>-0.03</sub> <sup>+1.30</sup>	2.60 <sub>-0.13</sub> <sup>+0.17</sup>
227	89.4	22.52 <sub>-0.02</sub> <sup>+0.12</sup>	11.2 <sub>-0.21</sub> <sup>+2.39</sup>	2.00 <sub>-0.01</sub> <sup>+0.02</sup>	21.21 <sub>-0.10</sub> <sup>+0.06</sup>	10.2 <sub>-0.10</sub> <sup>+1.29</sup>	2.05 <sub>-0.02</sub> <sup>+0.05</sup>	18.48 <sub>-0.20</sub> <sup>+0.07</sup>	9.11 <sub>-0.42</sub> <sup>+1.03</sup>	2.01 <sub>-0.12</sub> <sup>+0.16</sup>
277	84.9	23.14 <sub>-0.01</sub> <sup>+0.21</sup>	9.6 <sub>-0.14</sub> <sup>+0.33</sup>	2.08 <sub>-0.09</sub> <sup>+0.22</sup>	21.75 <sub>-0.05</sub> <sup>+0.05</sup>	8.7 <sub>-0.06</sub> <sup>+0.45</sup>	2.24 <sub>-0.17</sub> <sup>+0.30</sup>	19.02 <sub>-0.08</sub> <sup>+0.08</sup>	7.51 <sub>-0.38</sub> <sup>+1.07</sup>	2.02 <sub>-0.17</sub> <sup>+0.31</sup>
310	80.8	22.79 <sub>-0.04</sub> <sup>+0.08</sup>	9.9 <sub>-0.23</sub> <sup>+0.71</sup>	1.91 <sub>-0.04</sub> <sup>+0.10</sup>	21.19 <sub>-0.14</sub> <sup>+0.01</sup>	8.7 <sub>-0.29</sub> <sup>+0.63</sup>	1.95 <sub>-0.08</sub> <sup>+0.11</sup>	18.20 <sub>-0.28</sub> <sup>+0.10</sup>	7.31 <sub>-0.62</sub> <sup>+1.42</sup>	1.70 <sub>-0.13</sub> <sup>+0.17</sup>
349	117.6	22.21 <sub>-0.06</sub> <sup>+0.08</sup>	8.2 <sub>-0.46</sub> <sup>+0.64</sup>	1.63 <sub>-0.04</sub> <sup>+0.07</sup>	21.09 <sub>-0.14</sub> <sup>+0.05</sup>	7.5 <sub>-0.34</sub> <sup>+0.55</sup>	1.71 <sub>-0.07</sub> <sup>+0.11</sup>	18.68 <sub>-0.21</sub> <sup>+0.02</sup>	6.90 <sub>-0.06</sub> <sup>+0.50</sup>	1.75 <sub>-0.09</sub> <sup>+0.18</sup>
395	109.3	22.95 <sub>-0.04</sub> <sup>+0.06</sup>	12.4 <sub>-0.09</sub> <sup>+1.93</sup>	1.67 <sub>-0.02</sub> <sup>+0.05</sup>	21.46 <sub>-0.03</sub> <sup>+0.05</sup>	10.6 <sub>-0.02</sub> <sup>+1.61</sup>	1.74 <sub>-0.02</sub> <sup>+0.03</sup>	18.18 <sub>-0.11</sub> <sup>+0.12</sup>	8.40 <sub>-1.06</sub> <sup>+4.48</sup>	1.42 <sub>-0.06</sub> <sup>+0.07</sup>
436	109.2	22.58 <sub>-0.00</sub> <sup>+0.09</sup>	9.8 <sub>-0.00</sub> <sup>+0.59</sup>	2.11 <sub>-0.02</sub> <sup>+0.10</sup>	21.06 <sub>-0.02</sub> <sup>+0.02</sup>	7.9 <sub>-0.16</sub> <sup>+0.37</sup>	2.11 <sub>-0.12</sub> <sup>+0.20</sup>	17.71 <sub>-0.14</sub> <sup>+0.14</sup>	5.60 <sub>-0.60</sub> <sup>+0.73</sup>	1.55 <sub>-0.15</sub> <sup>+0.14</sup>
446	88.2	22.43 <sub>-0.09</sub> <sup>+0.10</sup>	18.3 <sub>-0.57</sub> <sup>+2.68</sup>	3.14 <sub>-0.09</sub> <sup>+0.09</sup>	20.74 <sub>-0.08</sub> <sup>+0.08</sup>	14.7 <sub>-0.08</sub> <sup>+2.13</sup>	3.03 <sub>-0.08</sub> <sup>+0.08</sup>	16.64 <sub>-0.39</sub> <sup>+0.15</sup>	10.0 <sub>-0.72</sub> <sup>+1.81</sup>	1.89 <sub>-0.26</sub> <sup>+0.27</sup>
780	34.4	22.22 <sub>-0.03</sub> <sup>+0.04</sup>	15.7 <sub>-0.94</sub> <sup>+1.08</sup>	4.34 <sub>-0.61</sub> <sup>+0.81</sup>	21.41 <sub>-0.40</sub> <sup>+0.05</sup>	15.1 <sub>-0.95</sub> <sup>+0.48</sup>	4.96 <sub>-0.72</sub> <sup>+0.88</sup>	19.28 <sub>-0.02</sub> <sup>+0.00</sup>	14.7 <sub>-0.01</sub> <sup>+0.86</sup>	3.95 <sub>-0.04</sub> <sup>+0.01</sup>
901	131.2	22.30 <sub>-0.10</sub> <sup>+0.09</sup>	8.0 <sub>-0.48</sub> <sup>+1.16</sup>	1.72 <sub>-0.07</sub> <sup>+0.11</sup>	21.10 <sub>-0.04</sub> <sup>+0.04</sup>	7.9 <sub>-0.71</sub> <sup>+0.88</sup>	1.71 <sub>-0.12</sub> <sup>+0.15</sup>	18.71 <sub>-0.05</sub> <sup>+0.03</sup>	7.0 <sub>-0.29</sub> <sup>+0.44</sup>	1.52 <sub>-0.03</sub> <sup>+0.02</sup>
913	62.5	21.98 <sub>-0.08</sub> <sup>+0.17</sup>	9.7 <sub>-0.60</sub> <sup>+1.02</sup>	1.60 <sub>-0.09</sub> <sup>+0.14</sup>	21.04 <sub>-0.17</sub> <sup>+0.08</sup>	9.0 <sub>-0.60</sub> <sup>+0.81</sup>	1.73 <sub>-0.10</sub> <sup>+0.14</sup>	18.91 <sub>-0.03</sub> <sup>+0.05</sup>	9.30 <sub>-0.03</sub> <sup>+0.39</sup>	1.86 <sub>-0.07</sub> <sup>+0.02</sup>
979	52.0	21.35 <sub>-0.10</sub> <sup>+0.15</sup>	13.0 <sub>-0.18</sub> <sup>+2.57</sup>	2.84 <sub>-0.24</sub> <sup>+0.26</sup>	20.27 <sub>-0.08</sub> <sup>+0.08</sup>	12.1 <sub>-0.27</sub> <sup>+1.18</sup>	3.03 <sub>-0.23</sub> <sup>+0.23</sup>	17.51 <sub>-0.29</sub> <sup>+0.06</sup>	11.1 <sub>-0.01</sub> <sup>+1.52</sup>	2.53 <sub>-0.22</sub> <sup>+0.32</sup>
1043	50.1	21.94 <sub>-0.05</sub> <sup>+0.08</sup>	20.7 <sub>-2.28</sub> <sup>+3.01</sup>	3.38 <sub>-0.14</sub> <sup>+0.20</sup>	20.59 <sub>-0.03</sub> <sup>+0.05</sup>	16.9 <sub>-1.07</sub> <sup>+0.38</sup>	3.43 <sub>-0.17</sub> <sup>+0.31</sup>	16.91 <sub>-0.39</sub> <sup>+0.22</sup>	10.6 <sub>-1.88</sub> <sup>+1.22</sup>	2.23 <sub>-0.36</sub> <sup>+0.36</sup>
1063	56.4	22.08 <sub>-0.01</sub> <sup>+0.12</sup>	7.8 <sub>-0.23</sub> <sup>+0.53</sup>	2.21 <sub>-0.10</sub> <sup>+0.05</sup>	21.19 <sub>-0.16</sub> <sup>+0.10</sup>	7.0 <sub>-0.17</sub> <sup>+0.51</sup>	2.22 <sub>-0.12</sub> <sup>+0.10</sup>	19.17 <sub>-0.07</sub> <sup>+0.07</sup>	7.41 <sub>-0.02</sub> <sup>+1.50</sup>	2.18 <sub>-0.10</sub> <sup>+0.01</sup>
1285	18.8	21.99 <sub>-0.06</sub> <sup>+0.25</sup>	22.6 <sub>-0.53</sub> <sup>+1.20</sup>	6.05 <sub>-0.63</sub> <sup>+0.55</sup>	20.99 <sub>-0.11</sub> <sup>+0.26</sup>	19.7 <sub>-0.71</sub> <sup>+1.74</sup>	6.63 <sub>-0.75</sub> <sup>+0.61</sup>	18.59 <sub>-0.09</sub> <sup>+0.10</sup>	15.8 <sub>-2.31</sub> <sup>+0.10</sup>	5.15 <sub>-0.23</sub> <sup>+0.29</sup>
1303	51.7	22.57 <sub>-0.02</sub> <sup>+0.34</sup>	9.2 <sub>-0.35</sub> <sup>+0.83</sup>	2.32 <sub>-0.24</sub> <sup>+0.35</sup>	21.70 <sub>-0.02</sub> <sup>+0.28</sup>	8.5 <sub>-0.40</sub> <sup>+0.67</sup>	2.50 <sub>-0.24</sub> <sup>+0.30</sup>	19.55 <sub>-0.11</sub> <sup>+0.02</sup>	5.81 <sub>-0.06</sub> <sup>+1.17</sup>	2.56 <sub>-0.10</sub> <sup>+0.18</sup>
1415	38.3	21.79 <sub>-0.04</sub> <sup>+0.31</sup>	19.1 <sub>-0.73</sub> <sup>+1.88</sup>	3.84 <sub>-0.40</sub> <sup>+0.56</sup>	20.83 <sub>-0.37</sub> <sup>+0.05</sup>	18.30 <sub>-1.18</sub> <sup>+0.39</sup>	4.27 <sub>-0.54</sub> <sup>+0.69</sup>	18.34 <sub>-0.18</sub> <sup>+0.01</sup>	15.3 <sub>-0.00</sub> <sup>+1.43</sup>	3.21 <sub>-0.15</sub> <sup>+0.29</sup>
1440	70.9	22.04 <sub>-0.07</sub> <sup>+0.02</sup>	19.7 <sub>-1.36</sub> <sup>+2.05</sup>	2.74 <sub>-0.10</sub> <sup>+0.15</sup>	20.54 <sub>-0.20</sub> <sup>+0.05</sup>	15.90 <sub>-0.15</sub> <sup>+0.86</sup>	2.78 <sub>-0.23</sub> <sup>+0.22</sup>	16.81 <sub>-0.26</sub> <sup>+0.12</sup>	10.2 <sub>-1.00</sub> <sup>+1.61</sup>	1.83 <sub>-0.15</sub> <sup>+0.15</sup>
1642	36.6	22.60 <sub>-0.04</sub> <sup>+0.10</sup>	12.2 <sub>-0.85</sub> <sup>+1.16</sup>	3.04 <sub>-0.13</sub> <sup>+0.12</sup>	21.76 <sub>-0.24</sub> <sup>+0.01</sup>	12.5 <sub>-0.14</sub> <sup>+1.32</sup>	3.53 <sub>-0.26</sub> <sup>+0.33</sup>	19.94 <sub>-0.04</sub> <sup>+0.07</sup>	18.5 <sub>-5.11</sub> <sup>+5.02</sup>	3.14 <sub>-0.08</sub> <sup>+0.05</sup>
1948	36.9	22.67 <sub>-0.03</sub> <sup>+0.27</sup>	13.1 <sub>-0.87</sub> <sup>+1.40</sup>	2.70 <sub>-0.26</sub> <sup>+0.27</sup>	21.86 <sub>-0.22</sub> <sup>+0.04</sup>	12.30 <sub>-0.44</sub> <sup>+0.51</sup>	2.98 <sub>-0.25</sub> <sup>+0.24</sup>	19.76 <sub>-0.00</sub> <sup>+0.10</sup>	8.70 <sub>-2.92</sub> <sup>+0.06</sup>	2.31 <sub>-0.00</sub> <sup>+0.01</sup>
2131	41.7	22.51 <sub>-0.08</sub> <sup>+0.08</sup>	10.7 <sub>-0.33</sub> <sup>+1.53</sup>	3.15 <sub>-0.13</sub> <sup>+0.18</sup>	21.30 <sub>-0.10</sub> <sup>+0.03</sup>	10.0 <sub>-0.32</sub> <sup>+1.06</sup>	3.46 <sub>-0.16</sub> <sup>+0.18</sup>	18.62 <sub>-0.05</sub> <sup>+0.05</sup>	8.90 <sub>-0.03</sub> <sup>+0.28</sup>	3.06 <sub>-0.03</sub> <sup>+0.10</sup>
2135	125.3	22.31 <sub>-0.04</sub> <sup>+0.06</sup>	7.6 <sub>-0.29</sub> <sup>+1.00</sup>	1.67 <sub>-0.02</sub> <sup>+0.00</sup>	21.06 <sub>-0.15</sub> <sup>+0.06</sup>	6.90 <sub>-0.23</sub> <sup>+0.67</sup>	1.73 <sub>-0.09</sub> <sup>+0.08</sup>	18.08 <sub>-0.14</sub> <sup>+0.05</sup>	4.80 <sub>-0.20</sub> <sup>+0.28</sup>	1.51 <sub>-0.06</sub> <sup>+0.09</sup>
2369	59.8	22.75 <sub>-0.07</sub> <sup>+0.17</sup>	8.8 <sub>-0.34</sub> <sup>+1.11</sup>	1.90 <sub>-0.12</sub> <sup>+0.21</sup>	21.81 <sub>-0.30</sub> <sup>+0.03</sup>	8.70 <sub>-0.50</sub> <sup>+0.62</sup>	2.14 <sub>-0.16</sub> <sup>+0.32</sup>	19.80 <sub>-0.06</sub> <sup>+0.02</sup>	9.51 <sub>-0.21</sub> <sup>+1.27</sup>	2.09 <sub>-0.04</sub> <sup>+0.04</sup>
2548	55.6	22.75 <sub>-0.05</sub> <sup>+0.23</sup>	10.7 <sub>-0.03</sub> <sup>+1.54</sup>	2.17 <sub>-0.15</sub> <sup>+0.30</sup>	21.65 <sub>-0.24</sub> <sup>+0.02</sup>	9.9 <sub>-0.05</sub> <sup>+0.87</sup>	2.43 <sub>-0.19</sub> <sup>+0.29</sup>	19.39 <sub>-0.19</sub> <sup>+0.00</sup>	9.60 <sub>-0.01</sub> <sup>+0.76</sup>	2.51 <sub>-0.09</sub> <sup>+0.27</sup>
2558	73.8	22.29 <sub>-0.03</sub> <sup>+0.03</sup>	9.8 <sub>-0.21</sub> <sup>+1.27</sup>	3.06 <sub>-0.02</sub> <sup>+0.03</sup>	21.27 <sub>-0.18</sub> <sup>+0.02</sup>	9.2 <sub>-0.44</sub> <sup>+1.00</sup>	3.15 <sub>-0.24</sub> <sup>+0.14</sup>	19.05 <sub>-0.05</sub> <sup>+0.05</sup>	9.11 <sub>-0.45</sub> <sup>+1.41</sup>	2.82 <sub>-0.12</sub> <sup>+0.13</sup>
E1371	82.6	23.02 <sub>-0.10</sub> <sup>+0.14</sup>	8.7 <sub>-1.07</sub> <sup>+1.51</sup>	2.12 <sub>-0.02</sub> <sup>+0.08</sup>	21.12 <sub>-0.10</sub> <sup>+0.02</sup>	7.7 <sub>-0.44</sub> <sup>+1.04</sup>	2.07 <sub>-0.04</sub> <sup>+0.03</sup>	17.06 <sub>-0.19</sub> <sup>+0.02</sup>	6.80 <sub>-0.25</sub> <sup>+0.19</sup>	1.47 <sub>-0.09</sub> <sup>+0.12</sup>
E1404	76.2	22.60 <sub>-0.04</sub> <sup>+0.06</sup>	8.9 <sub>-0.53</sub> <sup>+0.67</sup>	1.58 <sub>-0.03</sub> <sup>+0.03</sup>	21.36 <sub>-0.23</sub> <sup>+0.05</sup>	7.8 <sub>-0.12</sub> <sup>+0.68</sup>	1.64 <sub>-0.10</sub> <sup>+0.12</sup>	18.76 <sub>-0.18</sub> <sup>+0.12</sup>	7.0 <sub>-0.84</sub> <sup>+0.54</sup>	1.64 <sub>-0.11</sub> <sup>+0.13</sup>
E1498	135.5	22.48 <sub>-0.10</sub> <sup>+0.04</sup>	8.3 <sub>-0.21</sub> <sup>+1.89</sup>	1.48 <sub>-0.02</sub> <sup>+0.10</sup>	21.03 <sub>-0.01</sub> <sup>+0.12</sup>	7.6 <sub>-0.05</sub> <sup>+1.51</sup>	1.51 <sub>-0.04</sub> <sup>+0.09</sup>	17.50 <sub>-0.01</sub> <sup>+0.01</sup>	6.70 <sub>-0.35</sub> <sup>+0.38</sup>	1.11 <sub>-0.07</sub> <sup>+0.14</sup>
E1623	261.1	22.70 <sub>-0.04</sub> <sup>+0.08</sup>	7.9 <sub>-0.08</sub> <sup>+0.85</sup>	1.35 <sub>-0.02</sub> <sup>+0.03</sup>	21.07 <sub>-0.10</sub> <sup>+0.01</sup>	6.4 <sub>-0.07</sub> <sup>+0.18</sup>	1.25 <sub>-0.04</sub> <sup>+0.05</sup>	17.37 <sub>-0.17</sub> <sup>+0.08</sup>	4.50 <sub>-0.20</sub> <sup>+0.28</sup>	0.96 <sub>-0.07</sub> <sup>+0.06</sup>

<sup>1</sup> These fits use Equations 2 and 3 with  $N = 1$  (i.e. a  $\text{sech}^2$  vertical profile). Peak edge-on surface brightnesses have not been corrected for inclination. When available, distances taken from Karachentsev et al. (2000). Otherwise, we have used the recessional velocity corrected for Local Group infall to the Virgo cluster (LEDA). Throughout, we assume  $H_0 = 70 \text{ km s}^{-1} \text{ Mpc}^{-1}$ .

TABLE 4  
 VERTICAL LIGHT PROFILES FOR THE TWO DISK MODELS USED IN FITTING *R*-BAND STRUCTURAL PARAMETERS.

Thin disk model	Thick disk model	Notes
$\text{sech}^2(z/z_0)$	$\text{sech}^2(z/z_0)$	convolved w/1'' FWHM Gaussian
$\text{sech}^2(z/z_0)$	$\text{sech}^2(z/z_0)$	midplane masked
$\text{sech}^2(z/z_0)$	$\text{sech}^2(z/z_0)$	
$\text{sech}(z/z_0)$	$\text{sech}^2(z/z_0)$	
$\text{sech}^2(z/z_0)$	$\text{sech}(z/z_0)$	
$\text{sech}(z/z_0)$	$\text{sech}(z/z_0)$	

TABLE 5  
VERTICAL LIGHT PROFILES FOR THE TWO DISK MODELS USED IN FITTING *R*-BAND STRUCTURAL PARAMETERS.

FGC	Thin Disk			Thick Disk			$L_{thick}/L_{thin}$	n converged
	$\mu(0,0)$ (mag/ $\square''$ )	$h_r$ ( $''$ )	$z_0$ ( $''$ )	$\mu(0,0)$ (mag/ $\square''$ )	$h_r$ ( $''$ )	$z_0$ ( $''$ )		
31	$22.0^{+0.40}_{-0.03}$	$8.0^{+0.7}_{-4.2}$	$1.7^{+0.0}_{-0.60}$	$23.8^{+0.57}_{-0.13}$	$11.8^{+0.1}_{-0.6}$	$2.9^{+0.6}_{-0.8}$	$0.40^{+0.00}_{-0.16}$	3
36	$22.2^{+0.53}_{-0.21}$	$6.8^{+0.1}_{-0.5}$	$1.0^{+0.5}_{-0.3}$	$21.4^{+0.13}_{-0.13}$	$7.4^{+0.0}_{-0.1}$	$1.9^{+0.0}_{-0.1}$	$4.20^{+1.71}_{-3.46}$	4
130	$21.1^{+0.92}_{-0.03}$	$8.6^{+0.4}_{-0.2}$	$1.6^{+0.4}_{-0.2}$	$24.1^{+0.68}_{-1.31}$	$9.5^{+1.1}_{-1.0}$	$3.9^{+1.1}_{-1.8}$	$0.25^{+0.08}_{-0.14}$	5
164	$22.4^{+0.63}_{-0.04}$	$9.5^{+0.1}_{-0.5}$	$1.5^{+0.4}_{-0.4}$	$23.7^{+1.00}_{-0.17}$	$12.2^{+0.2}_{-1.4}$	$4.7^{+1.0}_{-1.3}$	$0.72^{+0.30}_{-0.44}$	5
215	$21.3^{+0.16}_{-0.00}$	$10.3^{+0.0}_{-0.3}$	$1.4^{+0.0}_{-0.3}$	$22.1^{+0.83}_{-0.90}$	$12.1^{+0.0}_{-0.9}$	$2.8^{+0.0}_{-0.7}$	$0.23^{+0.23}_{-0.05}$	3
225	$21.3^{+2.43}_{-0.00}$	$7.6^{+0.0}_{-2.3}$	$2.1^{+0.0}_{-1.4}$	$21.3^{+2.63}_{-0.00}$	$8.5^{+0.6}_{-0.8}$	$3.8^{+0.6}_{-1.3}$	$0.39^{+0.00}_{-0.24}$	3
227	$21.3^{+0.91}_{-0.12}$	$10.8^{+1.0}_{-0.8}$	$1.8^{+0.5}_{-0.2}$	$22.7^{+1.07}_{-0.74}$	$10.1^{+2.2}_{-0.8}$	$3.9^{+0.1}_{-1.4}$	$0.26^{+0.12}_{-0.19}$	5
277	$21.9^{+0.59}_{-0.12}$	$8.0^{+0.3}_{-0.1}$	$1.7^{+0.7}_{-0.1}$	$23.5^{+0.95}_{-0.34}$	$11.3^{+1.6}_{-0.8}$	$4.5^{+1.0}_{-0.8}$	$0.47^{+0.32}_{-0.24}$	5
310	$21.3^{+0.17}_{-0.00}$	$8.4^{+0.0}_{-0.6}$	$1.6^{+0.0}_{-0.3}$	$22.5^{+0.21}_{-0.00}$	$9.6^{+0.0}_{-0.5}$	$2.9^{+0.0}_{-0.0}$	$0.55^{+0.17}_{-0.14}$	3
349	$21.2^{+0.85}_{-0.01}$	$7.0^{+0.2}_{-0.4}$	$1.4^{+0.4}_{-0.5}$	$22.3^{+0.46}_{-0.80}$	$7.3^{+0.0}_{-0.1}$	$2.4^{+0.2}_{-0.5}$	$0.62^{+2.05}_{-0.20}$	5
395	$21.3^{+0.20}_{-0.00}$	$11.0^{+0.0}_{-0.7}$	$1.6^{+0.0}_{-0.3}$	$24.8^{+0.38}_{-0.00}$	$11.2^{+0.0}_{-0.4}$	$6.4^{+0.0}_{-0.2}$	$0.07^{+0.03}_{-0.02}$	3
436	$21.1^{+0.66}_{-0.04}$	$7.3^{+0.3}_{-0.1}$	$1.7^{+0.7}_{-0.1}$	$23.0^{+1.62}_{-0.15}$	$9.9^{+2.9}_{-0.1}$	$4.2^{+1.9}_{-0.4}$	$0.40^{+0.10}_{-0.29}$	5
446	$20.8^{+0.08}_{-0.16}$	$14.5^{+0.5}_{-0.0}$	$2.9^{+0.0}_{-0.2}$	$23.9^{+0.52}_{-0.49}$	$16.2^{+5.4}_{-0.6}$	$4.6^{+2.9}_{-0.2}$	$0.14^{+0.43}_{-0.05}$	4
780	$21.6^{+0.63}_{-0.07}$	$13.4^{+0.7}_{-0.4}$	$3.1^{+1.3}_{-0.4}$	$22.6^{+0.58}_{-0.13}$	$16.1^{+1.3}_{-0.3}$	$8.4^{+0.4}_{-1.1}$	$0.93^{+0.57}_{-0.34}$	5
901	$21.2^{+0.07}_{-0.14}$	$6.9^{+0.1}_{-0.1}$	$1.3^{+0.1}_{-0.2}$	$23.1^{+0.24}_{-0.96}$	$8.8^{+0.3}_{-0.1}$	$2.9^{+0.3}_{-0.6}$	$0.39^{+0.02}_{-0.06}$	4
913	$21.2^{+0.65}_{-0.22}$	$7.8^{+1.0}_{-0.5}$	$1.4^{+0.4}_{-0.1}$	$22.4^{+0.54}_{-0.01}$	$9.1^{+0.8}_{-0.5}$	$2.5^{+0.4}_{-0.1}$	$0.52^{+0.13}_{-0.14}$	5
979	$20.2^{+0.76}_{-0.08}$	$11.9^{+0.2}_{-0.5}$	$2.3^{+1.0}_{-0.8}$	$21.7^{+1.21}_{-0.69}$	$13.0^{+0.7}_{-0.6}$	$5.1^{+0.2}_{-1.2}$	$0.67^{+0.82}_{-0.49}$	5
1043	$20.8^{+0.05}_{-0.11}$	$19.3^{+0.0}_{-1.1}$	$2.7^{+0.0}_{-0.1}$	$22.3^{+0.57}_{-0.17}$	$11.3^{+1.7}_{-0.5}$	$6.9^{+0.5}_{-0.8}$	$0.33^{+0.06}_{-0.21}$	5
1063	$22.3^{+0.04}_{-1.32}$	$4.8^{+0.1}_{-0.1}$	$0.8^{+0.4}_{-0.1}$	$21.5^{+0.01}_{-0.12}$	$7.3^{+0.4}_{-0.2}$	$2.4^{+0.0}_{-0.1}$	$6.91^{+4.69}_{-1.65}$	4
1285	$21.2^{+0.29}_{-0.05}$	$17.3^{+1.6}_{-1.2}$	$4.4^{+0.7}_{-0.3}$	$22.2^{+0.58}_{-0.02}$	$23.6^{+1.8}_{-1.0}$	$10.1^{+0.6}_{-0.7}$	$1.08^{+1.00}_{-0.45}$	5
1303	$22.2^{+0.52}_{-0.06}$	$7.9^{+0.0}_{-1.4}$	$1.4^{+0.7}_{-0.3}$	$22.4^{+0.53}_{-0.13}$	$9.0^{+0.3}_{-0.3}$	$3.3^{+0.3}_{-0.3}$	$1.93^{+1.82}_{-1.03}$	5
1415	$20.9^{+0.63}_{-0.30}$	$15.0^{+0.6}_{-1.6}$	$2.8^{+1.0}_{-0.5}$	$22.1^{+0.68}_{-0.07}$	$21.1^{+1.6}_{-1.3}$	$6.6^{+0.8}_{-0.4}$	$0.95^{+0.36}_{-0.43}$	5
1440	$20.6^{+0.05}_{-0.02}$	$15.7^{+0.4}_{-0.3}$	$2.3^{+0.1}_{-0.1}$	$22.7^{+0.11}_{-0.16}$	$17.2^{+0.1}_{-0.2}$	$5.0^{+0.1}_{-0.2}$	$0.38^{+0.17}_{-0.05}$	4
1642	$21.8^{+0.58}_{-0.16}$	$11.6^{+0.4}_{-0.4}$	$3.1^{+0.8}_{-0.4}$	$24.6^{+0.65}_{-1.05}$	$19.5^{+0.9}_{-4.7}$	$10.0^{+1.3}_{-4.0}$	$0.19^{+0.33}_{-0.08}$	5
1948	$22.5^{+0.69}_{-0.50}$	$10.1^{+0.8}_{-0.4}$	$1.6^{+0.5}_{-0.3}$	$22.4^{+0.07}_{-0.06}$	$13.0^{+0.5}_{-0.3}$	$3.6^{+0.0}_{-0.1}$	$3.56^{+2.22}_{-1.00}$	4
2131	$21.3^{+0.22}_{-0.00}$	$9.3^{+0.2}_{-0.7}$	$2.8^{+0.1}_{-0.8}$	$22.7^{+0.88}_{-0.38}$	$10.5^{+1.3}_{-0.1}$	$4.9^{+1.3}_{-0.5}$	$0.29^{+0.33}_{-0.00}$	4
2135	$21.2^{+0.21}_{-0.09}$	$6.5^{+0.7}_{-0.7}$	$1.1^{+0.4}_{-0.8}$	$22.3^{+1.62}_{-0.29}$	$8.5^{+0.1}_{-0.29}$	$2.5^{+0.3}_{-0.1}$	$0.88^{+0.79}_{-0.67}$	4
2369	$22.2^{+0.52}_{-0.40}$	$8.3^{+0.1}_{-0.5}$	$1.4^{+0.6}_{-0.0}$	$23.3^{+0.14}_{-0.44}$	$9.3^{+0.2}_{-1.0}$	$3.4^{+0.2}_{-0.4}$	$0.75^{+0.46}_{-0.21}$	3
2548	$21.9^{+0.05}_{-0.08}$	$9.9^{+0.1}_{-0.1}$	$1.4^{+0.2}_{-0.1}$	$22.6^{+0.09}_{-0.12}$	$9.8^{+0.0}_{-0.0}$	$3.5^{+0.1}_{-0.1}$	$1.18^{+0.76}_{-0.14}$	4
2558	$21.8^{+0.06}_{-0.56}$	$8.4^{+1.3}_{-0.7}$	$2.6^{+0.1}_{-0.4}$	$22.4^{+0.93}_{-0.41}$	$10.1^{+0.0}_{-0.2}$	$3.6^{+1.2}_{-0.0}$	$0.47^{+1.31}_{-0.17}$	4
E1371	$21.2^{+0.91}_{-0.12}$	$8.6^{+0.3}_{-1.2}$	$1.6^{+0.7}_{-0.0}$	$22.9^{+0.17}_{-0.49}$	$7.3^{+0.1}_{-1.4}$	$3.4^{+0.0}_{-0.7}$	$0.27^{+0.37}_{-0.04}$	5
E1404	$21.6^{+1.09}_{-0.06}$	$6.8^{+0.2}_{-0.3}$	$1.3^{+0.1}_{-0.2}$	$22.4^{+0.26}_{-0.38}$	$9.2^{+0.4}_{-0.3}$	$2.2^{+0.1}_{-0.2}$	$1.12^{+2.04}_{-0.53}$	4
E1498	$20.9^{+0.11}_{-0.05}$	$7.7^{+0.3}_{-0.2}$	$1.2^{+0.2}_{-0.1}$	$23.8^{+0.35}_{-0.91}$	$8.3^{+0.2}_{-0.2}$	$3.8^{+0.4}_{-1.0}$	$0.19^{+0.05}_{-0.04}$	4
E1623	$21.3^{+0.11}_{-0.15}$	$6.4^{+0.1}_{-0.5}$	$0.9^{+0.2}_{-0.0}$	$22.5^{+0.23}_{-0.53}$	$6.3^{+0.1}_{-0.2}$	$1.8^{+0.0}_{-0.2}$	$0.53^{+0.20}_{-0.12}$	4